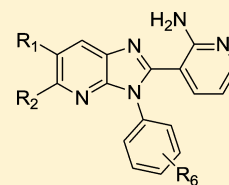


Discovery and Optimization of a Series of 3-(3-Phenyl-3*H*-imidazo[4,5-*b*]pyridin-2-yl)pyridin-2-amines: Orally Bioavailable, Selective, and Potent ATP-Independent Akt Inhibitors

Mark A. Ashwell, Jean-Marc Lapierre, Christopher Brassard, Karen Bresciano, Cathy Bull, Susan Cornell-Kennon, Sudharshan Eathiraj, Dennis S. France, Terence Hall, Jason Hill, Eoin Kelleher, Sampada Khanapurkar, Darin Kizer, Steffi Koerner, Jeff Link, Yanbin Liu, Sapna Makhija, Magdi Moussa, Nivedita Namdev, Khanh Nguyen, Robert Nicewonger, Rocio Palma, Jeff Szwaya, Manish Tandon, Uma Uppalapati, David Vensel, Laurie P. Volak, Erika Volckova, Neil Westlund, Hui Wu, Rui-Yang Yang, and Thomas C. K. Chan*

ArQule Inc., 19 Presidential Way, Woburn, Massachusetts 01801, United States

ABSTRACT: This paper describes the implementation of a biochemical and biophysical screening strategy to identify and optimize small molecule Akt1 inhibitors that act through a mechanism distinct from that observed for kinase domain ATP-competitive inhibitors. With the aid of an unphosphorylated Akt1 cocrystal structure of **12j** solved at 2.25 Å, it was possible to confirm that as a consequence of binding these novel inhibitors, the ATP binding cleft contained a number of hydrophobic residues that occlude ATP binding as expected. These Akt inhibitors potently inhibit intracellular Akt activation and its downstream target (PRAS40) *in vitro*. *In vivo* pharmacodynamic and pharmacokinetic studies with two examples, **12e** and **12j**, showed the series to be similarly effective at inhibiting the activation of Akt and an additional downstream effector (p70S6) following oral dosing in mice.



INTRODUCTION

Akt (protein kinase B or PKB) is a serine/threonine kinase that functions as a key signaling node in the PI3K/Akt/mTOR pathway and plays a central role in cell proliferation, migration, survival, and angiogenesis.¹ Oncogenic activation of Akt signal transduction has been described for a variety of human cancers, and it is therefore a compelling target for therapeutic intervention.² Akt1, Akt2, and Akt3 are three members of the Akt kinase family, each exhibiting specific patterns of expression in both normal and tumor tissues.³

Small molecule inhibitors of Akt are emerging with a few having advanced into clinical trials.⁴ With one notable exception⁵ most of the Akt inhibitors described to date are ATP-competitive and, because of the similarity of the ATP binding sites of the AGC kinase family, are generally poorly selective against closely related kinases. Furthermore they show little selectivity among the Akt isoforms.

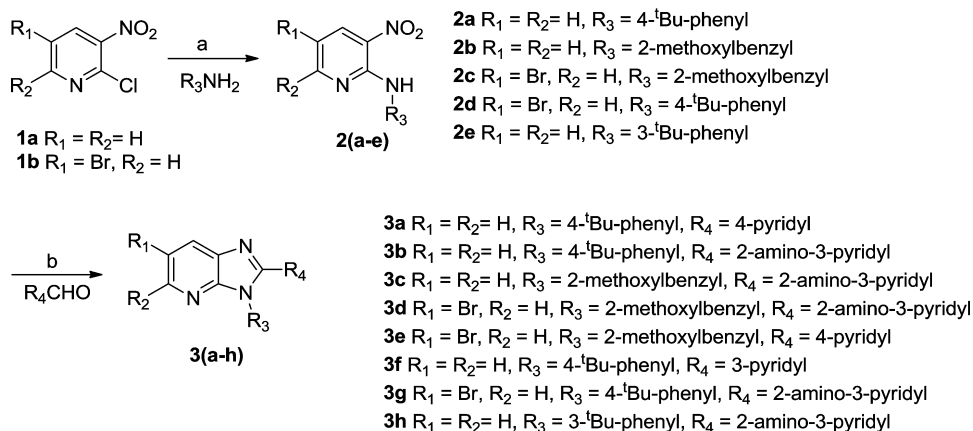
We recently described a novel inhibition mode for c-Met kinase⁶ that led to a new approach for the design and discovery of inhibitors that stabilize autoinhibited conformations of kinases.⁷ After characterization of the role of hydrophobic residues within the ATP-binding cleft in the autoinhibitory state, ATP-independent FGFR kinase inhibitors were identified and biologically characterized. Herein, we provide an expansion of this concept through the enablement of an *in silico* design and screening strategy to identify Akt1 inhibitors with an analogous mechanism of action. The goal was to identify inhibitors that utilized the intrinsic negative regulatory function of hydrophobic clusters in the ATP-binding cleft to inhibit the kinase activity of Akt1. The design and implementation of this

approach were customized to maximize the likelihood of identifying molecules exhibiting this mode of inhibition in the hit-generation phase of the program by utilizing a suite of biophysical and biochemical assays in parallel.

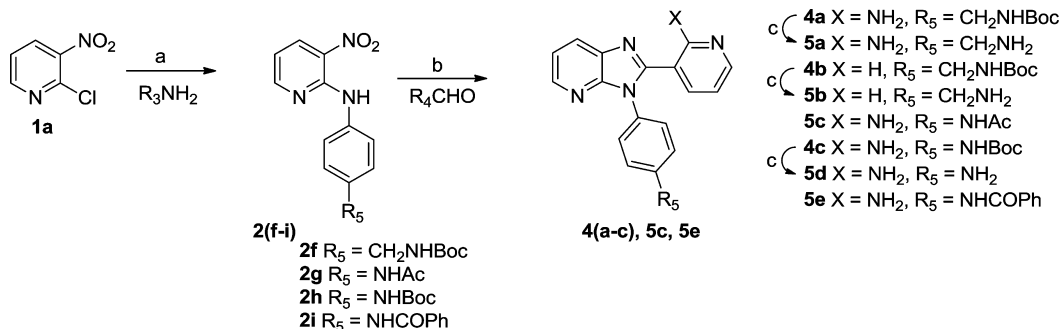
The Akt kinase family members, Akt1, Akt2, and Akt3, have three conserved domains, a N-terminal pleckstrin homology domain (PH domain), an ATP binding kinase domain, and a hydrophobic motif containing a C-terminal regulatory domain.⁸ While there is high homology between the catalytic kinase domains of the three Akt isoforms and other AGC family members, the unphosphorylated Akt2 isoform has been shown to adopt a very distinct inactive conformation compared to other AGC-kinase family members. In the published crystal structure of Akt2,⁹ there is a disordered α C-helix, and the ATP-binding cleft of Akt2 collapses into hydrophobic clusters that results in the steric occlusion of ATP from the binding site. It was hypothesized that the PH domain in Akt1 may play a role in stabilizing this inactive conformation. Indeed, unlike in Akt2, when a Lys-C limited proteolytic cleavage of Akt1 was attempted, it did not lead to a separable PH domain, indicating that the PH-domain stabilization of the unphosphorylated, inactive Akt1 was likely stronger than observed in Akt2. This suggested that maximal stabilization of the autoinhibited forms of Akt might necessitate the utilization of the full-length unphosphorylated forms of the enzymes. To optimally evaluate the ability of compounds to bind to Akt1 in the inactive state, several biophysical methods that included indirect affinity mass

Received: February 27, 2012

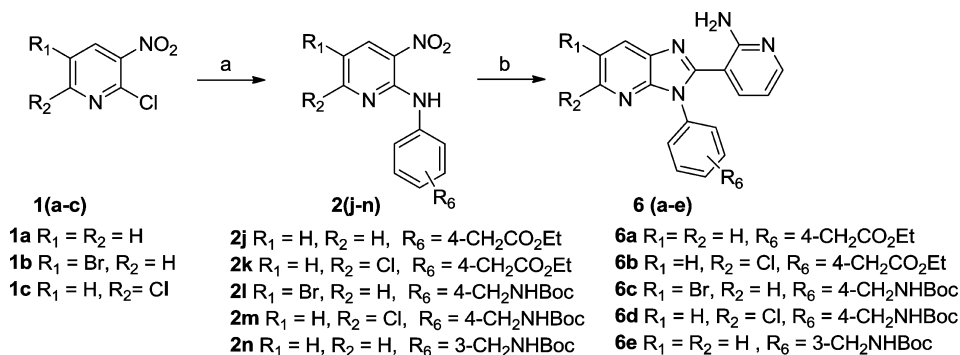
Published: April 25, 2012

Scheme 1^a

^aReagents and conditions: (a) $R_3\text{NH}_2$, DIEA, DMSO or 1,4-dioxane, 80 °C, overnight; (b) $R_4\text{CHO}$, $\text{Na}_2\text{S}_2\text{O}_4$, DMSO, MeOH, 100 °C, overnight.

Scheme 2^a

^aReagents and conditions: (a) anilines, DIEA, DMSO or 1,4-dioxane, 80 °C, overnight; (b) $R_4\text{CHO}$, $\text{Na}_2\text{S}_2\text{O}_4$, DMSO, MeOH, 100 °C, overnight; (c) 4.0 M HCl in 1,4-dioxane, 1,4-dioxane, room temperature, overnight.

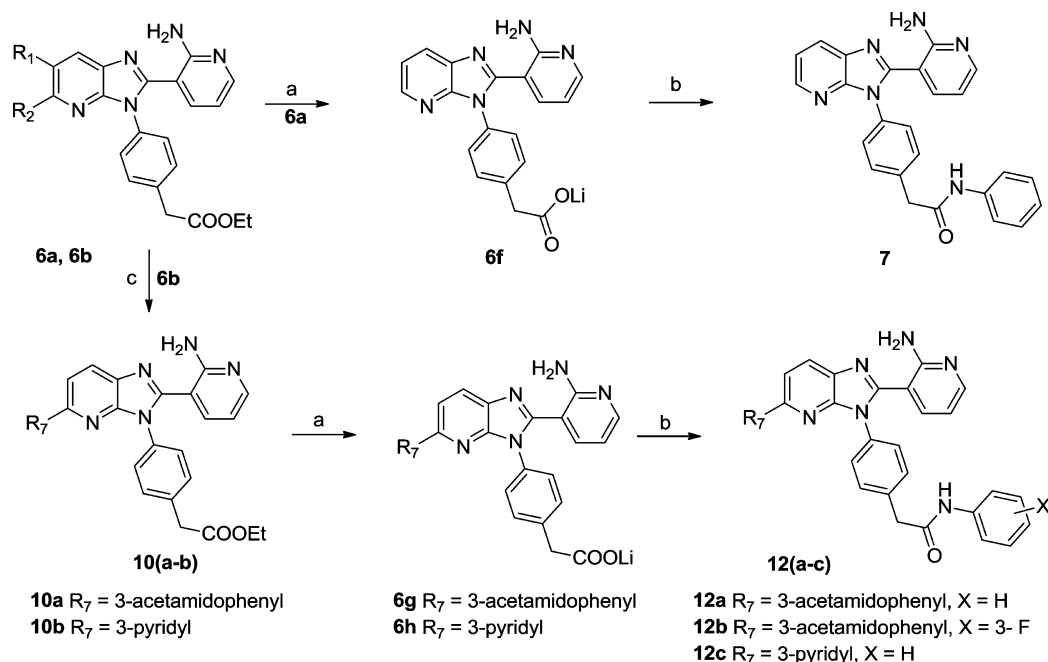
Scheme 3^a

^aReagents and conditions: (a) *tert*-butyl 4-aminobenzylcarbamate, *tert*-butyl 3-aminobenzylcarbamate or ethyl 2-(4-aminophenyl)acetate, 1,4-dioxane, diisopropylethylamine, 80 °C, overnight; (b) 2-aminonicotinaldehyde, $\text{Na}_2\text{S}_2\text{O}_4$ (85%), DMSO, MeOH, 100 °C, overnight.

spectrometry (IA-MS),¹⁰ thermal shift assay (TSA),^{11,12} and surface plasmon resonance (SPR)¹³ were employed.

In order to determine the functional consequence of stabilizing the autoinhibitory conformation, unphosphorylated full length Akt proteins were used in the Akt biochemical assays. Biochemical inhibition was determined following in situ activation after preincubation with test compounds. The activation of Akt involves translocation to the plasma membrane and binding to phosphoinositides. The interaction of phosphoinositides with the PH domain of Akt induces a conformational change that enables phosphorylation of Thr308

in the activation loop by the membrane-localized phosphoinositide-dependent kinase 1 (PDK1). Full activation of Akt requires phosphorylation of Ser473 on the HM domain by an upstream kinase, the mTORC2 complex.¹⁴ Therefore, the unphosphorylated full length protein constructs (Akt1 (1–480), Akt2 (1–481), and Akt3 (1–479)) were preincubated with potential inhibitors followed by the addition of the activating kinases PDK1 and MAPKAPK2 (a functional surrogate for mTORC2-mediated phosphorylation), lipid vesicles, and ATP prior to the addition of substrate. To remove the possibility that inhibitors of PDK1 and MAPKAK2 would complicate data analysis,

Scheme 4^a

^aReagents and conditions: (a) LiOH, THF–MeOH–H₂O, room temperature; (b) aniline or substituted anilines, HBTU, TEA, DMF, room temperature; (c) arylboronic acid, Pd(PPh₃)₄, saturated NaHCO₃ solution, toluene–ethanol, 100 °C, overnight.

counterscreens against these two kinases were employed.¹⁵ Finally, in the screening phase of the project, the activated catalytic domain (Akt1 (104–480)) was employed as a cross-screen.

■ SYNTHESIS

Starting from commercially available 2-chloro-3-nitropyridine (**1a**), 5-bromo-2-chloro-3-nitropyridine (**1b**), and 2,6-dichloro-3-nitropyridine (**1c**), 2-chloro displacement with the appropriate aniline in DMSO or dioxane with base provided compounds **2a–n** in good yields (Schemes 1–3). Compound **3a–h** (Scheme 1) were prepared by condensation of **2a–e** with the corresponding pyridylaldehydes. The one-pot reductive cyclization was carried out using sodium hydrosulfite in a mixture of DMSO and methanol at 100 °C. In a similar manner **4a–c**, **5c**, and **5e** (Scheme 2) were synthesized from intermediates **2f–i**. Removal of the boc protection from **4a**, **4b**, and **4c** was effected by treatment with 4 M HCl in dioxane at room temperature to provide **5a**, **5b**, and **5d**, respectively.

Intermediates **6a–e** (Scheme 3) were prepared using standard displacement and cyclization chemistry as described in Schemes 1 and 2.

As shown in Scheme 4, the two ester intermediates **6a** and **6b** were converted into phenylacetamides **7** and **12a–c**. Acid **6a** was first hydrolyzed to the lithium carboxylate salt **6f** which was subsequently coupled with aniline using HBTU to yield the amide **7**. Alternatively, the 5-chloro substituent of **6b** was reacted with either 3-acetamidophenylboronic acid or 3-pyridylboronic acid using a Suzuki reaction.^{16,17} Hydrolysis to the corresponding lithium salts **6g** and **6h** followed by coupling to the appropriate anilines gave the desired amides **12a–c**.

Boc protected aminomethyl intermediates **4a** and **6c–e** were converted into a series of amides and amines as shown in Schemes 5 and 6. Removal of the boc protecting group from **4a** and **6c–e** with 4 M HCl in dioxane provided the hydrochloride

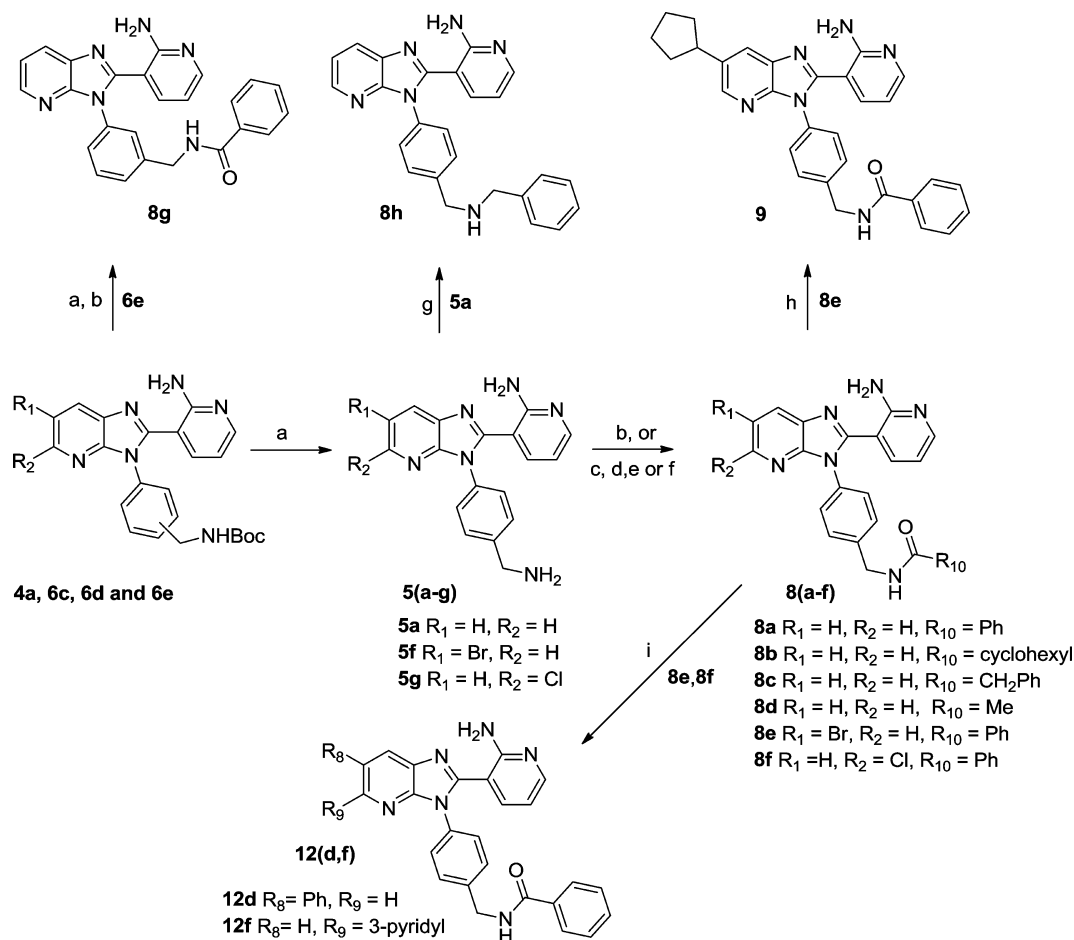
salts **5a**, **5f**, **5g**, and the intermediate for preparing **8g**. The ammonium intermediate **5a** was coupled with benzoic acid under standard HBTU conditions to provide amide **8a**. **8b** and **8c** were obtained using the appropriate acids and 1,1'-carbonyldiimidazole (CDI). Reaction of **5a** with acetyl chloride gave **8d**. **8e** was prepared by coupling **5f** with benzoic acid using 1-(3-dimethylaminopropyl)-3-ethylcarbodiimide (EDCI) as the coupling reagent. Finally, **5g** was converted into **8f** using benzoyl chloride in the presence of NaOH. Further modification of the halogen substituents of **8e** and **8f** using phenyl- or 3-pyridylboronic acids under standard Suzuki conditions gave **12d** and **12f**, respectively. Reductive amination of **5a** with benzaldehyde in the presence of tetramethylammonium triacetoxyborohydride provided amine **8h**. **9** was prepared from **8e** using zinc coupling. Reaction of **8e** with cyclopentylzinc bromide in the presence of Pd[P(^tBu)₃]₂ and potassium *tert*-butoxide in THF gave **9** in a modest yield.¹⁸

Amides **12e** and **12g–k** were prepared by reversing the sequence of Suzuki coupling and amide formation from that used for compounds **12d** and **12f**. The boc protected intermediates **4a**, **6c**, and **6d** (Scheme 6) provided **10c–f** following a Suzuki coupling reaction. Removal of the boc group gave the hydrochloride salts **11a–d** which were converted into the amides **12e** and **12g–k** using CDI as the coupling reagent and the corresponding acids.

■ RESULTS AND DISCUSSION

To demonstrate that ATP did not bind to the full length unphosphorylated Akt1 (1–480) and that a representative ATP-competitive inhibitor also did not bind to this form of the protein, binding affinity and biochemical inhibition were measured.

The ATP mimetic, AMP-PNP, did not bind to and/or stabilize the full length inactive Akt1 (Table 1), indicating that the protein is in a conformation that precludes ATP binding.

Scheme 5^a

^aReagents and conditions: (a) 4.0 M HCl in 1,4-dioxane, 1,4-dioxane, room temperature, overnight; (b) acids, HBTU, TEA, DMF, room temperature; (c) benzoic acid, 1,1'-carbonyldiimidazole, DMA, room temperature; (d) acetyl chloride, DIEA, DCM; (e) benzoic acid, 1-(3-dimethylaminopropyl)-3-ethylcarbodiimide hydrochloride, diisopropylethylamine, DCM, room temperature; (f) benzoyl chloride, NaOH, water, room temperature; (g) benzaldehyde, $\text{Me}_4\text{N}(\text{OAc})_3\text{BH}$, TEA, AcOH, DCE, room temperature, 20 h; (h) cyclopentylzinc bromide, $\text{Pd}(\text{P}^t\text{Bu}_3)_2$, KO^tBu , THF, microwave, 100 °C, 15 min; (i) arylboronic acid, $\text{Pd}(\text{PPh}_3)_4$, aqueous NaHCO_3 , ethanol-toluene, reflux, overnight.

Similarly, the ATP-competitive inhibitor A674563¹⁹ did not bind and/or stabilize the full length inactive Akt1, thereby providing additional support that the assays employing this form of Akt1 would be suitable for the identification of non-ATP competitive inhibitors. Both AMP-PNP and the ATP-competitive inhibitor showed stronger affinity for the unphosphorylated truncated kinase domain (residues 144–480) (Table 1).

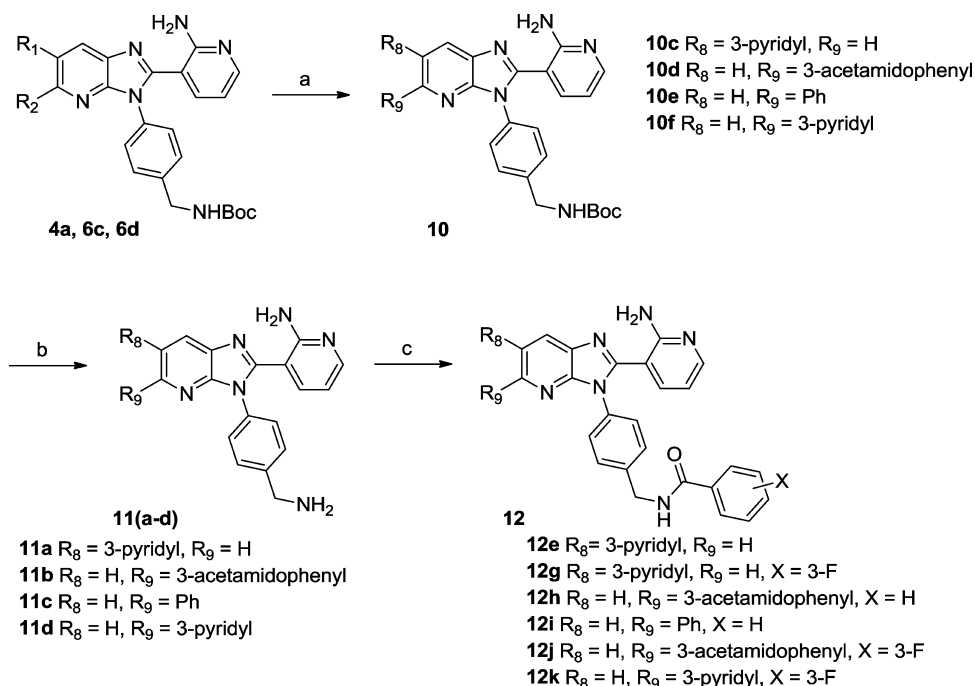
These data are consistent with the underlying assumption that the unphosphorylated full length Akt1 adopts an autoinhibitory conformation and that ligands that bind to and stabilize this conformation can be experimentally differentiated from ATP-competitive ligands.

While A674563 and AMP-PNP do not bind to the full length inactive Akt1 protein used in the biophysical assay (Table 1), A674563 is a biochemical inhibitor in the substrate phosphorylation assay employing the same full length inactive Akt1 protein. This indicates that in order for A674563 to show inhibition, the conformation of the Akt1 protein must change. As A674563 is an ATP-competitive inhibitor and the ATP mimic AMP-PNP does not bind to the full length inactive Akt1 protein, it is likely that the protein moves to an active conformation during the course of the biochemical assay so that

ATP can bind (and phosphorylate the substrate) and thus A674563 can compete for this conformation.

Initially we employed indirect affinity mass spectrometry (IA-MS) to identify binders to the unphosphorylated Akt1 (1–480) from our compound collection. The compounds selected for screening were from three distinct sources. Library 1 consisted of approximately 7000 members across multiple scaffolds selected to represent active kinase inhibitors (those most likely to be type 1 or type 2 inhibitors). The second library, library 2, comprised approximately 5000 members of multiple scaffolds designed to target inactive conformations of kinases other than type 2 inhibitor designs. The final collection of molecules (1000 members across more than 11 scaffolds) was designed in silico to be specifically tailored toward the stabilization of the inactive conformations of Akt1.²⁰

Compounds from libraries 1 and 2 were pooled and screened in mixtures of 20 compounds per well by the IA-MS technique, and the compounds binding to the protein were identified by their unique mass fingerprint using a hyphenated SEC/LC/MS protocol. This rapid screen resulted in the identification of more than 1200 binders. In order to provide a ranking of these binders, a confirmatory binding screen using a thermal shift assay was employed. From monitoring of the shift in the

Scheme 6^a

^aReagents and conditions: (a) arylboronic acid, Pd(PPh₃)₄, aqueous NaHCO₃, ethanol–toluene, reflux, overnight; (b) 4.0 M HCl in 1,4-dioxane, 1,4-dioxane, room temperature, overnight; (c) acids, 1,1'-carbonyldiimidazole, DMA, room temperature.

Table 1. Biochemical and Biophysical Results for Two Reference Compounds^a

ligand	thermal shift assay, Δ <i>T</i> _m (°C)		Trp fluorescence quench assay, <i>K</i> _d (μM)		biochemical assay, IC ₅₀ (μM) Akt1 (1–480)
	Akt1 (1–480)	Akt1 (144–480)	Akt1 (1–480)	Akt1 (144–480)	
AMP-PNP	no shift	1.9	NB ^b	3.3	>100
A674563	no shift	1.3	NB ^b	2.1	0.27

^aSee Experimental Section for assay details. The *T*_m shifts were measured at the following concentrations: AMP-PNP at 1.2 mM and A674563 at 15 μM. ^bNB = no binding.

protein melting temperature (*T*_m) in the presence and absence of the ligand, the degree of stabilization was determined. A shift greater than 0.6 °C in the protein *T*_m (3 × STD) was taken as indicative of compound binding. Previous studies have shown that the degree of stabilization correlates well with the binding affinity of the inhibitor. The *in silico* designed Akt1 library (library 3) was directly screened in the thermal shift assay.

From the combined thermal shift analysis, approximately 80 compounds were identified as stabilizers of the full length unphosphorylated form of Akt1 (Table 2). While the protein stabilization for these initial hits was generally modest (Δ*T*_m ≈ 1 °C), 11 distinct scaffolds were identified as stabilizers with low biochemical inhibition. In addition, several additional scaffolds contained a number of stabilizers of Akt for which no biochemical inhibition could be detected.

Scaffolds were prioritized for optimization, and four were advanced to the hit-to-lead stage of the project based on their binding and biochemical inhibition profile. Two out of the four selected scaffolds originated from library 2 and two from library 3.

Herein we describe the SAR and optimization of one of those scaffolds. Scaffold 24 contained several structurally related analogues including 2-(pyridinyl)-3*H*-imidazo[4,5-*b*]pyridine and 3-(3*H*-imidazo[4,5-*b*]pyridin-2-yl)pyridin-2-amine derivatives. By comparison of the thermal stabilization with

biochemical inhibition of both inactive and preactivated enzymes by these analogues, it was clear that the assays were providing differentiation at the substructure level.

This differentiation within scaffold 24 was clearly demonstrated by comparing the profiles of 3b (a 3-(3*H*-imidazo[4,5-*b*]pyridin-2-yl)pyridin-2-amine subseries member) and 3e (a 2-(pyridinyl)-3*H*-imidazo[4,5-*b*]pyridine subseries member). Relatively small structural modifications on the central 3*H*-imidazo[4,5-*b*]pyridine core provided quite distinct biological profiles against Akt1 (Table 3). For example, while 3b binds to (Δ*T*_m = 1.9 °C) and biochemically inhibits the full length Akt1 (IC₅₀ = 3.9 μM), the structurally related analogue 3e neither binds to nor inhibits Akt1. When 3b and 3e were tested for their inhibition of the preactivated kinase domain of Akt1 (104–480), 3e was an Akt1 inhibitor (IC₅₀ = 5.9 μM) while 3b did not show any appreciable inhibition (6.3% inhibition at 30 μM). The lack of inhibition of the preactivated kinase domain indicated that the subseries represented by 3b was inhibiting Akt1 in a manner distinct from that of ATP-competitive ligands.

In order to gain a better understanding of the structure–activity relationships (SARs) of scaffold 24, a small set of compounds were prepared in the hit-to-lead phase of the program (Table 3). Replacement of the 4-pyridine ring of 3e with the 2-aminopyridine ring of 3b gave 3d which did not bind

Table 2. Hit Generation Results^a

scaffold	library size	no. of TSA actives	no. of biochemical actives	Akt1 IC ₅₀ (μM)
1	1109	2	0	NA ^c
2	106	3	1	4.3–8.9
5	382	1	0	NA ^c
7	776	5	2	14–72
9	170	9	36	12–100
10	81	1	0	NA ^c
11	14	1	0	NA ^c
17	69	19	6	16–100
18	19	1	1	>100
19	8	2	2	16–100
20	20	7	5	9.4–100
22	6	2	0	NA ^c
24	313	2	1	1.5–16
28	15	1	3	50–100
29	9	1	1	>100
30	32	2	3	12–71
31	196	3	0	NA ^c
32	9	2	0	NA ^c
33 ^b	151	5	2	10–100
34 ^b	40	2	2	22–100

^aSee Experimental Section for assay details. ^bScaffolds from the in silico directed homology methodology. ^cNA = not active.

to or inhibit full length Akt1. As **3g** demonstrated binding to Akt1, albeit somewhat reduced ($\Delta T_m = 0.9$ °C), a negative effect on binding of the bromine substituent was ruled out in

Table 3. Akt1 Biochemical and Biophysical Results for Scaffold 24^a

Compd	R ₁	R ₃	R ₄	Akt1	
				ΔT_m (°C)	IC ₅₀ (μM)
3a	H			no shift	>300
3b	H			1.9	3.9
3c	H			no shift	58
3d	Br			no shift	>300
3e	Br			no shift	>300
3f	H			no shift	185
3g	Br			0.9	>300
3h	H			no shift	>300
5a	H			2.6	0.93
5b	H			no shift	8.8
5c	H			3.7	1.3
5d	H			4.1	0.74

^aSee Experimental Section for assay details. The compounds were tested at 30 μM in the thermal shift assay.

3d, although the reason for the lack of biochemical inhibition for **3g** was not apparent. Replacement of the 4-pyridine ring in **3e** with the 2-amino pyridine group provided **3c** which was also a nonbinder and more than a 10-fold weaker inhibitor than **3b**. In addition, comparison of **3a** and **3f**, which were both biophysically and biochemically inactive, further confirmed the importance of the 2-aminopyridine substituent on the 3H-imidazo[4,5-*b*]pyridine core. The importance of the para-substitution for activity was clearly demonstrated by **3h**. Movement of the *tert*-butyl group to the meta position resulted in a loss of all activity against Akt1.

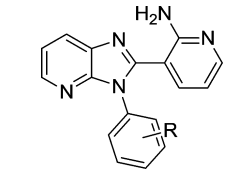
From these results, it was apparent that the screening paradigm employed had successfully separated two closely related series of Akt1 inhibitors by their mechanism of inhibition. The next objective was to increase the potency of the 2-(pyridinyl)-3H-imidazo[4,5-*b*]pyridine series, since this class of compounds met our screening requirements of binding to and preventing the activation of Akt1.

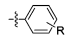
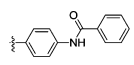
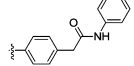
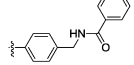
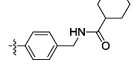
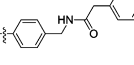
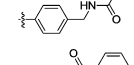
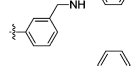
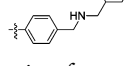
Having established a preference for para-substituents (compare **3h**, a nonbinder, to **3b**) on the pendent phenyl ring, replacement of the *tert*-butyl group was examined (Table 3). Compound **5d** indicated that the *tert*-butyl group could be replaced with a smaller more polar substituent, such as an aniline group, to provide a concomitant increase in both binding and biochemical inhibition ($\Delta T_m = 4.1$ °C which corresponds to a K_d of approximately 0.5 μM, IC₅₀ = 0.74 μM). The acetamide **5c** further demonstrated that this position could be modified, although no apparent improvement over **5d** was observed. Replacement of the undesirable aniline to the more polar benzylamine **5a** provided an improvement over **3b** with decreased protein stabilization when compared to the aniline **5d**. **5b** confirmed that the newly introduced benzylamine group also required the presence of the 2-amino group in the pyridine ring for binding and submicromolar inhibition. Its removal resulted in a loss of binding and a decrease in inhibition. Compared to **3b**, the acetamide **5c** had a 3-fold lower IC₅₀, and so additional amides were prepared. The benzamide group of **5e** (Table 4) increased the stabilization by more than 3 °C over the simple aniline **5d**, and similar improvements were observed for the benzylamide **8a** and the reverse amide **7**.

The steric requirements for this benzamide improvement in profile were further probed by analogues **8b**, **8h**, and **8c**, and in each case a decrease in activity compared to **5e** was observed. The loss in activity for the acetamide **8d** and the meta-positional isomer of **8a**, **8g**, showed clearly the sensitivity of this position to modification with a strong preference for an aromatic ring attached to the para-position with a short nonbasic linker.

Having identified **7** and **8a** as strong binders to Akt1 with IC₅₀ below 0.03 μM, a number of AGC-kinase family members were added to a minipanel screen together with representatives from CAMK, CMGC, STE, and TKs.²¹ At a screening concentration of 5 μM, **7** and **8a** showed no inhibition above 25% of any kinase in the panel, demonstrating their selectivity for Akt and providing support for the further optimization of the inhibitors.

To assess the isoform selectivity of the inhibitors, both binding affinity and biochemical inhibition were assessed using unphosphorylated forms of Akt2 (1–479) and Akt3 (1–481) proteins. These additional assays were employed in the lead optimization phase of the program to monitor the effect of chemical modification on the isoform selectivity. In vitro cellular activity was assessed in two cell lines, A2780 (ovarian)

Table 4. Akt1 Structure–Activity Relationship for Para-Substituents^a


Compd		Akt1	
		ΔT_m (°C)	IC_{50} (μM)
5e		7.3	0.014
7		7.9	0.028
8a		7.7	0.023
8b		5.7	0.25
8c		4.7	0.66
8d		2.3	0.81
8g		no shift	13
8h		4.9	0.26

^aSee Experimental Section for assay details. The compounds were tested at 30 μM in the thermal shift assay.

and AN3CA (endometrial), expressing all three Akt isoforms. The effects of the inhibitors on the phosphorylation of Ser473 and Thr308, and downstream Akt-mediated phosphorylation of PRAS40,²² were measured 2 h after treatment by Western blot analysis. Additionally, the inhibition of cellular proliferation in

the same cell lines was also assessed using a standard MTS assay.

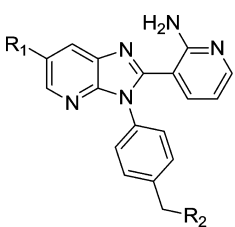
The initial results from the cell-based experiments to assess the ability of the compounds to inhibit phosphorylation of Akt were encouraging, as compounds of modest potency were able to induce cellular pharmacodynamic changes (Table 5). Both **8a** and **7** were cell-penetrant as shown by their ability to reduce the levels of phosphorylation of Ser473 and Thr308 in A2780 cells ($IC_{50} < 0.5 \mu M$). However, this did not result in an expected reduction of the phosphorylation of the downstream target PRAS40 ($IC_{50} > 10 \mu M$). In the AN3CA cells, both **8a** and **7** were approximately 10-fold less potent at inhibiting the phosphorylation of Ser473, and no significant inhibition of phosphorylation of Thr308 or PRAS40 ($IC_{50} > 10 \mu M$) was apparent. Additionally, both compounds failed to induce appreciable growth inhibition in either cell line. These data clearly suggested that increased in vitro potency against Akt1 and possibly Akt2 and/or Akt3 would be required if more pronounced cellular effects were to be obtained.²³

In order to achieve the necessary improvements in Akt inhibition, additional sites on the 3-(3*H*-imidazo[4,5-*b*]pyridin-2-yl)pyridin-2-amine core were modified (Table 6). It was found that a lipophilic substituent at the 6-position of the 3-(3-phenyl-3*H*-imidazo[4,5-*b*]pyridin-2-yl)pyridin-2-amine core generally improved binding to Akt isoforms, although some groups such as the cyclopentyl of **9** (Table 6) increased binding affinity to Akt2 rather than Akt1 when compared to **7** or **8a**. However, with a 3-pyridinyl substituent at the 6-position a substantial increase in Akt1 stabilization ($\Delta T_m = 9.2 \text{ }^\circ C$) and inhibition ($IC_{50} = 8 \text{ nM}$) was observed for **12e** when compared to **8a**. A similar increase in binding to Akt2 ($\Delta T_m = 4.8 \text{ }^\circ C$) resulted in a 22-fold increase in inhibition ($IC_{50} = 30 \text{ nM}$). Introduction of a meta-F group into the phenyl ring of the benzamide group of **12e** provided **12g**, which demonstrated a further increase in binding to Akt2 ($\Delta T_m = 5.4 \text{ }^\circ C$) with no significant change in the biochemical inhibition. As shown in Table 5, the two most potent 6-substituted analogues, **12e** and its meta-F analogue **12g**, were also potent cellular inhibitors of the activation of Akt (antibodies recognize all forms of the corresponding phospho-Akt) in both human cancer cell lines.

Table 5. Cellular Potency of Inhibitors^a

compd	p-Akt, IC_{50} (μM)							
	S473		T308		p-PRAS40 (T246), IC_{50} (μM)		MTS, IC_{50} (μM)	
	A2780	AN3CA	A2780	AN3CA	A2780	AN3CA	A2780	AN3CA
7	0.21	2.5	1.3	>10	>10	>10	57	70
8a	0.41	5.6	0.37	>10	>10	>10	>100	>100
8e	<0.012	2.5	0.17	>10	3.1	>10	65	60
9	0.27	3.7	0.21	9.4	2.1	>10	65	33
12a	0.046	0.047	0.054	0.049	0.31	>10	6.0	2.1
12b	0.12	0.09	0.015	0.26	0.14	1.5	3.3	1.7
12c	0.065	0.069	0.055	0.051	0.48	2.5	9.4	8.8
12d	0.33	0.16	0.68	1.1	1.8	0.98	>100	>100
12e	0.10	0.08	0.062	0.091	0.95	1.5	>100	>100
12f	0.034	1.4	0.067	4.2	0.74	3.2	23	13
12g	0.054	0.046	0.20	0.049	0.58	0.82	19	13
12h	0.13	0.11	0.14	0.17	0.91	0.84	1.6	1.5
12i	0.068	>10	0.18	>10	0.41	>10	9.5	5.5
12j	0.027	0.044	0.032	0.045	0.25	0.22	2.2	2.0
12k	0.19	0.095	0.69	0.34	1.3	2.1	10	10

^aSee Experimental Section for assay details.

Table 6. Structure–Activity Relationship of 6-Substituted Analogues^a


Compd	R ₁	R ₂	Akt1		Akt2		Akt3	
			ΔT _m (°C)	IC ₅₀ (μM)	ΔT _m (°C)	IC ₅₀ (μM)	ΔT _m (°C)	IC ₅₀ (μM)
7	H		6.7	0.028	1.2	0.70	no shift	22
8a	H		6.4	0.023	1.3	0.66	no shift	24
8e	Br		8.1	0.027	3.0	0.13	1.0	>10
9			6.0	0.11	3.3	0.80	no shift	>100
12d			5.61	0.033	1.2	51	no shift	>100
12e			9.2	0.008	4.8	0.030	1.6	0.66
12g			9.4	0.0052	5.4	0.027	1.5	0.40

^aSee Experimental Section for assay details. The compounds were tested at 15 μM in the thermal shift assay.

Specifically, **12e** demonstrated an approximately 70-fold decrease in IC₅₀ for the inhibition of phosphorylation of Ser473 (IC₅₀ = 80 nM) and marked improvement in the potency in inhibiting Thr308 phosphorylation (IC₅₀ = 91 nM) in the AN3CA cell line, compared to **8a** (IC₅₀ > 10 μM). A further improvement in cellular potency for **12g** compared to **12e** was observed in both cell lines. Additionally, it was also apparent that an aromatic 6-substituent (phenyl or 3-pyridyl) provided cellular inhibition of the downstream marker, phospho-PRAS40, in the AN3CA cancer cell line, the first time such a pharmacodynamic effect had been demonstrated in the campaign. However, this pharmacodynamic effect was not accompanied by a concomitant increase in antiproliferative potency. Indeed, the most potent 6-substituted Akt1 inhibitor in Table 6 (**12g** IC₅₀ = 5 nM) showed only modest (IC₅₀ > 10 μM, Table 5) activity in the cell proliferation assay in the two human cancer cell lines.

The in vitro ADME profile of **12e** (Table 7) was satisfactory with good microsomal stability and a lack of CYP450 inhibition. Despite the weak effect on cellular proliferation, **12e** was selected for proof-of-concept pharmacokinetic and pharmacodynamic studies in vivo.

In a mouse pharmacokinetic study (oral dose at 100 mg/kg, iv at 2.5 mg/kg), **12e** was well absorbed with good oral bioavailability (*F* = 46%). For the pharmacodynamic assessment, NCr-M nude mice were implanted with AN3CA tumor

xenografts, and the inhibition of the phosphorylation of Akt as well as the downstream kinase p70S6 (Thr389) was evaluated following treatment with the inhibitor. In addition, tumor and plasma samples were collected and the concentration of **12e** was determined. As shown in Table 8, 2 h after oral solution

Table 8. In Vivo Pharmacokinetic and Pharmacodynamic Results For 12e and 12j^a

compd	po dose (mg/kg)	time (h)	% inhibition			plasma concn (μM)	tumor concn (μM)
			p-Akt (S473)	p-Akt (T308)	p-p70S6 (T389)		
12e	100	2	82	25	76	14.1	8.4
12j	250	2	62	57	90	2.0	1.2
		4	51	67	86	1.2	0.6

^aSee Experimental Section for assay details.

dosing at 100 mg/kg, **12e** reduced the phosphorylation of Akt (Ser473) by 82% and the phosphorylation of p70S6 by 76% in tumors. Plasma levels of **12e** at the 2 h time point were 14.1 μM with the tumor concentrations slightly lower (8.4 μM). These positive results demonstrated that this chemical series could provide a selective Akt1 inhibitor with good druglike properties capable of inhibiting pharmacodynamic markers in vivo following oral delivery. However, the lack of cellular potency in the AN3CA MTS assay (IC₅₀ > 100 μM) needed to be addressed in order to demonstrate in vivo tumor growth inhibition.

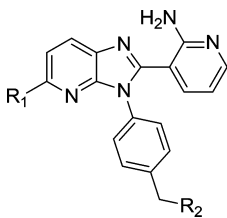
Increasing the inhibition of cellular proliferation became the goal of the next phase of optimization and was achieved by the introduction of substituents at the 5-position of the 3-(3-phenyl-3*H*-imidazo[4,5-*b*]pyridin-2-yl)pyridin-2-amine core (Table 9). This proved to be a very effective strategy for achieving dramatic improvements in Akt1 binding as shown by the range of *T_m* values (increase in Δ*T_m* from 9.7 to 13.0 °C), a significant increase compared to the 6-positional isomers. Interestingly, in most cases this did not directly translate into a similar increase in the Akt1 biochemical potency as had been observed with the 5-substituents. For example, **12j** had the same Akt1 biochemical inhibition as **12g** (IC₅₀ = 5 nM), yet the Δ*T_m* upon binding of **12j** was 13 °C compared to the 9.4 °C for **12g**. A similar trend was also apparent for Akt2, a possible explanation for which is discussed below.

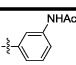
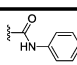
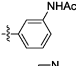
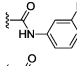
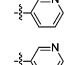
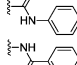
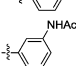
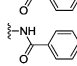
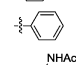
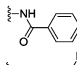
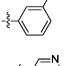
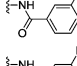
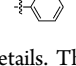
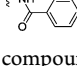
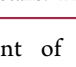
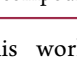
The crystal structure of nonphosphorylated Akt1 (1–446) was solved in complex with **12j** to assist the SAR optimization.²⁴ In the cocrystal structure the N-terminal PH domain and the C-terminal kinase domains were tightly associated in a “closed” conformation (Figure 1A). The overall structure of Akt1 is similar to a reported crystal structure of Akt1 (1–443) bound to an allosteric inhibitor which was published²⁵ during the course of this work. Crucially, however,

Table 7. In Vitro ADME Properties of Selected Compounds^a

compd	CYP 450, IC ₅₀ (μM)						liver microsomal stability at 1.0 μM, <i>T</i> _{1/2} (min)		
	1A2	2C19	2C8	2C9	2D6	3A4	HLM	MLM (F)	MLM (M)
7	>10	>10	>10	>10	>10	>10	47.6	>60	>60
8a	>10	>10	>10	>10	>10	>10	60	>60	>60
12e	>10	>10	>10	>10	>10	>10	>30	>60	>60
12j	>10	1–10	1–10	1–10	>10	>10	>30	>30	>30

^aSee Experimental Section for assay details.

Table 9. Structure–Activity Relationship of 5-Substituted Analogues^a


Compd	R ₁	R ₂	Akt1		Akt2		Akt3	
			ΔTm (°C)	IC ₅₀ (μM)	ΔTm (°C)	IC ₅₀ (μM)	ΔTm (°C)	IC ₅₀ (μM)
12a			11.4	0.016	6.5	0.015	1.7	0.7
12b			11.1	0.017	6.7	0.024	1.5	2.5
12c			10.8	0.05	5.1	0.025	1.8	0.39
12f			9.7	0.028	4.0	0.032	1.0	0.37
12h			12.8	0.015	6.7	0.047	2.5	0.17
12i			11.0	0.024	6.4	0.035	1.8	0.39
12j			13.0	0.005	7.7	0.018	2.9	0.17
12k			11.1	0.047	5.7	0.08	1.6	0.66

^aSee Experimental Section for assay details. The compounds were tested at 15 μM in the thermal shift assay.

the important structural element of this work, the 2-aminopyridine group of the (3-phenyl-3*H*-imidazo[4,5-*b*]pyridin-2-yl)pyridin-2-amine core, makes direct hydrogen bond interactions with the loop of β4 which are distinctly different. Additionally the αC-helix of the kinase domain is disordered.

As expected, the kinase domain adopts a DFG-out conformation similar to the inactive form of the Akt2 catalytic domain structure. The activation loop in the kinase domain is displaced outward because of a direct interaction of the PH domain which is in an inward orientation with the C-lobe such that the phosphoinositide binding region is buried at the interface. **12j** is bound at an allosteric pocket formed between the kinase domain and the PH domain. The ATP-binding region is occupied with nonpolar residues which are associated as tight clusters. The cleft is closed with a “hydrophobic lock” which may function to sterically exclude the binding of both ATP and ATP-competitive inhibitors (Figure 1B). The interdomain interactions stabilize the autoinhibitory conformation of Akt1 which is likely induced by **12j** binding, as the majority of the inhibitor is buried in a groove between the PH and kinase domains. The conserved tryptophan (Trp80) in the PH domain makes a key hydrophobic interaction with the core of **12j**, and the ring-nitrogen is bridged to the aspartic acid residue of the DFG-motif by a water molecule mediated hydrogen bond network. The plane of the imidazopyridine ring of the core is hydrophobically stacked between Trp80 and the E-helix residues Val270 and Leu264 (Figure 1C).

Solving the structure with **12j** assisted in the SAR optimization of this and other series of Akt1 inhibitors. The position of hydrogen donor and acceptor groups present within the 2-aminopyridine moiety of the 3-(3*H*-imidazo[4,5-*b*]pyridin-2-yl)pyridin-2-amine is critical for the inhibitor interaction. Removal of the amine and/or moving the pyridine

nitrogen around the aromatic ring disrupts this and leads to a loss of binding (Table 3). The plane of the pendent phenyl ring is perpendicular to the core and forms a direct hydrophobic interaction with the conserved Tyr272 residue of the AGC family.

Visual inspection of the cocrystal structure shows that substituents other than those at the para position will be detrimental to binding. In addition, the amide linker does not participate in any direct interaction with Akt1. Rather, it functions to orientate the terminal phenyl ring for a hydrophobic interaction with Ile84 of the PH domain. This likely explains the need for an additional hydrophobic ring for optimal binding and inhibition and a rationale as to why there is little preference for the amide or reverse amide (Table 4). The improved binding of the 5-substituents over the 6-substituents and the preference for the phenylacetamide group in the meta-position are due to a combination of complementary matching of the phenyl ring with a nonpolar region, which is made up of the aliphatic side chains of several amino acid residues, and a direct hydrogen bond interaction of the carbonyl of the phenylacetamide with the NH main chain atoms of the Trp80 residue.

A rationalization of the observed Akt isoform binding specificity for these inhibitors is apparent also. The Val270 residue provides a hydrophobic interaction with the core (Figure 1C). In Akt2, this residue is also valine, while in Akt3 the corresponding residue is the sterically larger isoleucine (Figure 1D). The additional methyl group in Akt3 is expected to require a reorientation in order to bind the inhibitors in a similar manner.

The cocrystal structure of **12j** bound to Akt 1 shows that the inhibitor occupies a deep cavity at the interface of kinase and the PH domains. A tight network of inhibitor interactions with Akt suggests that the binding requires extensive rearrangement

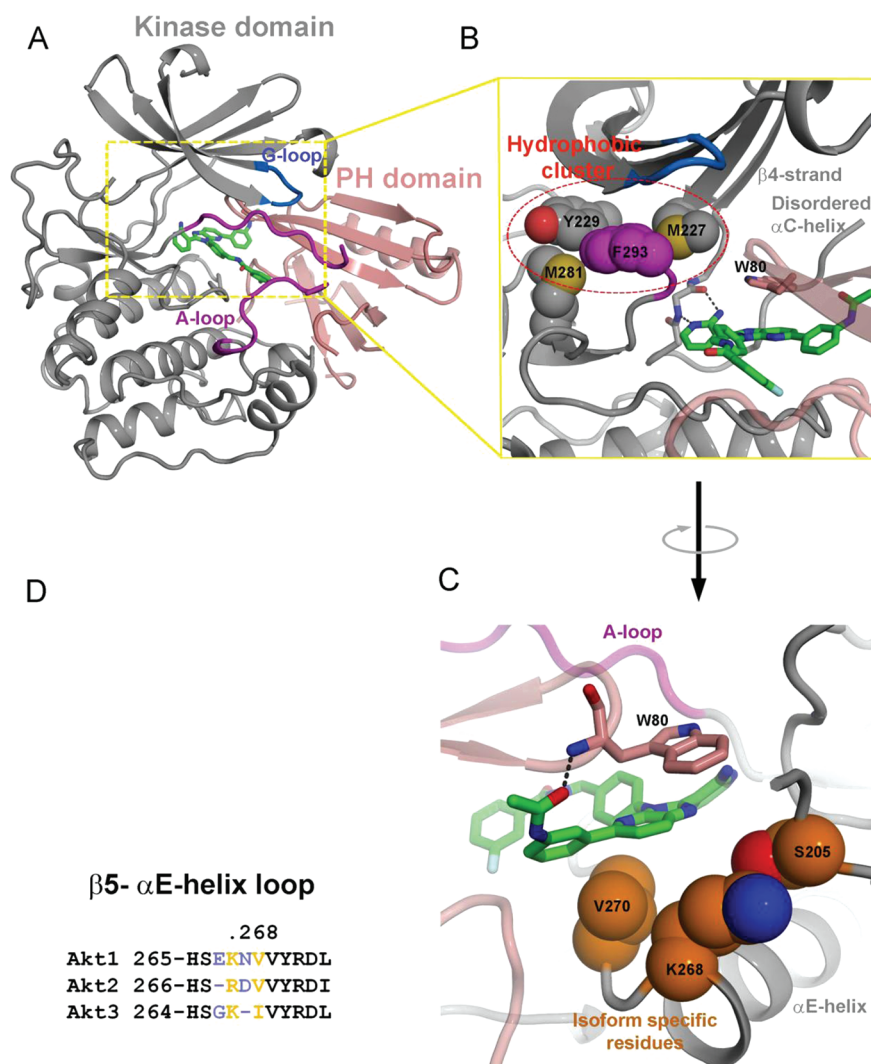


Figure 1. Cocystal structure of Akt1 (2–446) in complex with **12j** (PDB accession code 4EJN). (A) **12j** binds deep in the cavity between the kinase and PH domains and bridges the two domains with extensive polar and nonpolar interactions. The tight association of the PH domain with the kinase domain prevents the A-loop from adopting an active conformation. (B) A close view of the ATP binding region is shown to indicate the hydrophobic residues organized into hydrophobic clusters with steric exclusion of ATP binding in the cleft. **12j** binds beneath the hydrophobic clusters, and the aminopyridyl group binds to the loop of the β 4-strand and α C-helix through hydrogen bonding interactions. The plane of imidazopyridine core is matched to that of the indole ring of Trp80 of the PH domain. (C) Sequence alignment of the Akt isoform in a region that may play a role in isoform specificity. (D) The side chain of Val270 essentially complements the hydrophobic interaction with the aromatic core of **12j**. Substitution of Val270 with Ile as in Akt3 is likely to have a negative impact on Akt3 binding, favoring Akt1 and Akt2 selectivity.

of residues at the interface that facilitates binding of the inhibitor deeply between the interdomains. The impact of this conformational change upon binding was measured by following the kinetics of the interaction using SPR. A slow on-rate ($3.7 \times 10^4 \text{ M}^{-1} \text{ s}^{-1}$) and off-rate ($1.0 \times 10^{-4} \text{ s}^{-1}$) indicate strong binding of **12j** to Akt1 ($k_{\text{off}}/k_{\text{on}} = 2.7 \text{ nM}$), which is in agreement with the large thermal stabilization of 13°C measured by the thermal shift assay. The measured on-rate is several orders of magnitude lower than the rate of a diffusion governed process, suggesting that the binding likely induces a large conformational rearrangement in Akt1. This is consistent with the structural data and may contribute to the contraction of the dynamic range of the biochemical assay for the most potent binders of the 5-substituted analogues. The mechanism of action of **12j** with Akt1 was studied with respect to ATP. **12j** showed mixed uncompetitive/noncompetitive type kinetics with respect to ATP. In addition the inhibition of Akt1 by **12j** was compared to that of the ATP-competitive ligand A674563

by determining the fold decrease in IC_{50} with increasing concentrations of ATP (up to 1 mM) (Figure 2). As expected, the fold decrease is considerably less with **12j**, as is to be expected with its mechanistic profile.

On the basis of the *in vitro* biochemical profile, the stronger binding affinity, its slow off-rate, and superior cellular pharmacodynamic profile (especially in AN3CA cells), **12j** was advanced into broader kinase panel screening and further *in vivo* studies.

In a broad kinase panel screen of 297 kinases, **12j** showed excellent Akt selectivity with no kinase being inhibited at greater than 17%.²⁶ *In vitro* ADME profiling results (Table 7) showed **12j** to have good microsomal stability and a reasonable CYP450 inhibition profile. An oral solution formulation of **12j** allowed a dosing at 250 mg/kg , and two time points (2 and 4 h) were selected for plasma and tumor sampling. As shown in Table 8, the inhibition of phosphorylation of the downstream marker p70S6 was excellent at both time points (90% at 2 h

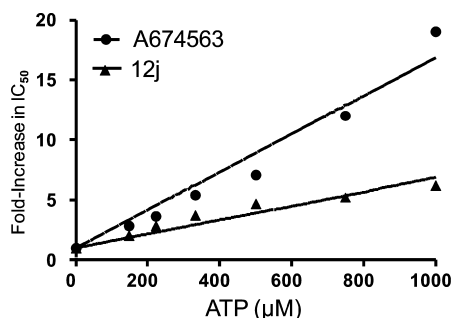


Figure 2. Inhibition of Akt1 by 12j and the ATP competitive inhibitor A674563 as a function of ATP concentration.

and 86% at 4 h) as was the degree of inhibition of pAkt(Thr308) (57% at 2 h, 67% at 4 h). The inhibition of pAkt(Ser473) was also robust, albeit somewhat less pronounced than had been observed for 12e. Unfortunately, the measured plasma and tumor concentrations of 12j at both time points were low especially compared to the concentrations observed for 12e which had been dosed at the lower level of 100 mg/kg. The final phase of the optimization was then focused upon improving the druglike properties of these potent and selective Akt inhibitors.

In conclusion, through the implementation of a screening paradigm designed to thoroughly annotate Akt1 kinase inhibitors by their mode of inhibition, a novel series of Akt1 inhibitors were discovered and advanced through lead optimization. SAR-guided optimization of the selected series using in vitro biophysical and biochemical assessment provided highly selective Akt inhibitors. In vivo characterization employed both pharmacokinetic and pharmacodynamic analyses and characterized lead inhibitors as orally bioavailable, well tolerated with robust inhibition of the activation of Akt as well as a downstream substrate, p70S6. Further optimization of this series is anticipated to yield additional biologically active Akt inhibitors with antitumor activity in appropriate animal models and will be detailed in the near future.

EXPERIMENTAL SECTION

Chemistry. All reagents and solvents were purchased from commercially available sources and used without further purification. All reactions were carried out according to the indicated procedures and conditions. Reactions were monitored by LC/MS analysis and/or thin-layer chromatography (TLC) on silica-coated glass plates (EMD silica gel 60 F₂₅₄) with the indicated eluent. The compounds were visualized by UV light (254 nm). LC/MS analysis was performed on a Shimadzu HPLC/UV (214 nm and/or 254 nm wavelength) system coupled to ELSD (Sedex 75, Sedere) and MS (ZQ, Micromass) detectors. Compounds were dissolved in 100% DMSO and separated on Zorbax SB-C8 rapid resolution cartridge (30 mm × 4.6 mm, 3.5 μm, 3 mL/min flow rate) using acetonitrile/water mobile phase with 0.1% TFA as a modifier. The gradient started at 5% acetonitrile and linearly increased to 95% acetonitrile in 1.9 min, with 0.3 min hold at 95% and re-equilibration to the original conditions in a total of 2.5 min. The purity of the compounds selected for in vivo studies was determined using an Agilent HP1100 system with a YMC C18 column (4.6 mm × 100 mm, 5 μm, 1 mL/min flow rate) and acetonitrile/water mobile phase with 0.1% TFA modifier. The gradient started at 2% acetonitrile, linearly increased to 30% acetonitrile in 7 min, followed by a linear increase to 80% acetonitrile by 12 min and a hold at 80% by 16 min. Purity was determined at 254 nm wavelength as >95%. Library compounds were purified by reverse phase chromatography on a preparative LC/UV/MS system (high throughput purification) using a mass triggered fractionation method. Compounds

were eluted from the HPLC column (Maccel 120-10-C18 SH, 10 μm, 20 mm i.d. × 50 mm) at 88 mL/min with an acetonitrile/water gradient using 0.1% TFA as a modifier. Nuclear magnetic resonance (¹H NMR) spectra were recorded on a Varian Mercury plus NMR spectrometer operating at 400.13 MHz frequencies for ¹H, using a 5 mm ASW PFG probe capable of detecting ¹H, ¹³C, ³¹P, ¹⁵N nuclei. The proton chemical shifts (ppm) were referenced to the tetramethylsilane standard (0 ppm). NMR data are reported with these descriptions: s, singlet; d, doublet; t, triplet; q, quartet; m, multiplet; br, broad peak.

N-(4-(tert-Butyl)phenyl)-3-nitropyridin-2-amine (2a). 2-Chloro-3-nitropyridine **1a** (1.0 g, 6.31 mmol), 4-(tert-butyl)aniline (1.0 g, 6.72 mmol), and DIEA (1.74 mL, 10.0 mmol) in DMSO (20 mL) were stirred at 80 °C for 16 h. DMSO was removed under reduced pressure to give a brown solid (2.2 g) which was purified by column chromatography (1% MeOH/DCM, silica gel) to give **2a** (1.55 g, 89%) as a red solid. Mp 156–158 °C. ¹H NMR (400 MHz, DMSO-*d*₆) δ 9.92 (s, 1H), 8.51 (dd, *J* = 14.5, 5.6 Hz, 1H), 7.54 (d, *J* = 8.4 Hz, 1H), 7.38 (d, *J* = 8.5 Hz, 1H), 6.96 (dd, *J* = 8.1, 4.6 Hz, 1H), 1.29 (s, 9H). MS *m/z* 272 [M + H]⁺.

N-(4-((3-Nitropyridin-2-yl)amino)phenyl)acetamide (2g). **2g** was prepared from **1a** as described for **2a** using *N*-(4-aminophenyl)acetamide. Mp 177–180 °C. ¹H NMR (400 MHz, DMSO-*d*₆) δ 9.93 (s, 1H), 9.91 (s, 1H), 8.50 (dd, *J* = 8.3, 1.8 Hz, 1H), 8.47 (dd, *J* = 4.5, 1.8 Hz, 1H), 7.53 (d, *J* = 2.4 Hz, 4H), 6.93 (dd, *J* = 8.3, 4.5 Hz, 1H), 2.02 (s, 9H). MS *m/z* 273 [M + H]⁺.

tert-Butyl 4-((3-Nitropyridin-2-yl)amino)phenylcarbamate (2h). **2h** was prepared from **1a** as described for **2a** using *tert*-butyl (4-aminophenyl)carbamate. Mp 162–165 °C. ¹H NMR (400 MHz, DMSO-*d*₆) δ 9.88 (s, 1H), 9.32 (s, 1H), 8.50 (dd, *J* = 8.2, 1.8 Hz, 1H), 8.45 (dd, *J* = 4.5, 1.7 Hz, 1H), 7.48 (d, *J* = 9.0 Hz, 2H), 7.41 (d, *J* = 8.9 Hz, 2H), 6.92 (dd, *J* = 8.4, 4.5 Hz, 1H), 1.46 (s, 9H). MS *m/z* 331 [M + H]⁺.

tert-Butyl 4-((5-Bromo-3-nitropyridin-2-yl)amino)benzylcarbamate (2l). **2l** was prepared from 2-chloro-3-nitro-5-bromopyridine (**1b**) as described for **2a** using *tert*-butyl 4-aminobenzylcarbamate. Mp 178–180 °C. ¹H NMR (400 MHz, DMSO-*d*₆) δ 9.95 (s, 1H), 8.65 (m, 1H), 8.54 (s, 1H), 7.51 (d, *J* = 6.4 Hz, 2H), 7.23 (d, *J* = 6.4 Hz, 2H), 4.21–4.12 (m, 2H), 1.41 (s, 9H). MS *m/z* 423 [M + H]⁺.

tert-Butyl 4-((6-Chloro-3-nitropyridin-2-yl)amino)benzylcarbamate (2m). **2m** was prepared as described for **2a** using 2-chloro-3-nitro-6-chloropyridine (**1c**) and *tert*-butyl 4-aminobenzylcarbamate. Mp 103–106 °C. ¹H NMR (400 MHz, CDCl₃) δ 10.24 (s, 1H), 8.45 (d, *J* = 8.6 Hz, 1H), 7.60 (d, *J* = 6.2 Hz, 2H), 7.31 (d, *J* = 8.2 Hz, 2H), 6.79 (d, *J* = 8.6 Hz, 1H), 4.31 (d, *J* = 5.8 Hz, 2H), 1.46 (s, 9H). MS *m/z* 379 [M + H]⁺.

3-(4-(tert-Butyl)phenyl)-2-(pyridine-4-yl)-3H-imidazo[4,5-*b*]pyridine (3a). *N*-(4-(tert-Butyl)phenyl)-3-nitropyridin-2-amine **2a** (1.52 g, 5.6 mmol), isonicotinaldehyde (0.82 g, 7.61 mmol), sodium dithionite (2.45 g, 14.1 mmol), methanol (15 mL), and DMSO (15 mL) were combined. The mixture was shaken at 100 °C for 18 h. The methanol was removed under reduced pressure. The solution was diluted with DMSO (40 mL) and H₂O (40 mL) and filtered to yield a brown solid (2.2 g). Purification by column chromatography (100% DCM to 5% MeOH/DCM, silica gel) gave **3a** (0.76 g, 41%) as a pale yellow solid. Mp 184–186 °C. ¹H NMR (400 MHz, DMSO-*d*₆) δ 8.62 (dd, *J* = 3.8, 2.0 Hz, 2H), 8.39 (dd, *J* = 3.3, 1.4 Hz, 1H), 8.29 (dd, *J* = 3.4, 2.0 Hz, 1H), 7.59 (d, *J* = 8.4 Hz, 2H), 7.49 (dd, *J* = 3.8, 2.1 Hz, 2H), 7.44 (dd, *J* = 5.0, 3.0 Hz, 1H), 7.40 (d, *J* = 8.4 Hz, 2H), 1.35 (s, 9H). MS *m/z* 329 [M + H]⁺. Anal. Calcd for C₂₁H₂₀N₄: C, 76.8; H, 6.14; N, 17.06. Found: C, 76.53; H, 6.15; N, 17.13.

3-(1-(4-(tert-Butyl)phenyl)-1H-benzo[*d*]imidazol-2-yl)pyridin-2-amine (3b). **3b** was prepared as described for **3a** using **2a** and 2-aminonicotinaldehyde. Mp 175–180 °C. ¹H NMR (400 MHz, acetone-*d*₆) δ 8.44–8.42 (dd, *J* = 4.7, 1.2 Hz, 1H), 8.26–8.23 (dd, *J* = 8.2, 1.6 Hz, 1H), 8.05–8.02 (dd, *J* = 6.3, 1.6 Hz, 1H), 7.75–7.73 (dd, *J* = 7.8, 1.6 Hz, 1H), 7.70–7.68 (dd, *J* = 6.6, 2.3 Hz, 2H), 7.57–7.55 (dd, *J* = 8.6, 1.9 Hz, 2H), 7.48–7.44 (dd, *J* = 8.2, 4.7 Hz, 1H), 6.82–6.78 (dd, *J* = 7.8, 6.3 Hz, 1H), 1.41 (s, 9H). MS *m/z* 344 [M + H]⁺.

Anal. Calcd for $C_{21}H_{21}N_5 \cdot 1.5TFA \cdot 0.1$ acetone: C, 56.10; H, 4.48; N, 13.46. Found: C, 56.32; H, 4.25; N, 13.70.

3-(3-(2-Methoxybenzyl)-3H-imidazo[4,5-b]pyridin-2-yl)pyridin-2-amine (3c). Step 1: *N*-(2-Methoxybenzyl)-3-nitropyridin-2-amine (**2b**) was prepared as described for **2a** using **1a** and (2-methoxyphenyl)methanamine. Step 2: **3c** was prepared from **2b** as described for **3a** using 2-aminonicotinaldehyde. Mp 175–182 °C. 1H NMR (400 MHz, acetone- d_6) δ 9.2 (s, 1H), 8.48–8.46 (dd, $J = 4.7, 1.6$ Hz, 1H), 8.20–8.16 (dd, $J = 7.8, 1.2$ Hz, 1H), 8.14–8.07 (m, 2H), 7.43–7.40 (dd, $J = 7.8, 4.7$ Hz, 1H), 7.28–7.24 (m, 1H), 7.03–6.97 (dd, $J = 9.0, 0.78$ Hz, 2H), 6.89–6.86 (dd, $J = 1.6, 0.7$ Hz, 1H), 6.83–6.79 (m, 1H), 5.7 (s, 2H), 3.8 (s, 3H). MS m/z 332 [M + H] $^+$. Anal. Calcd for $C_{19}H_{17}N_5O \cdot 1.22TFA \cdot 0.5$ acetone: C, 54.78; H, 3.94; N, 14.79. Found: C, 54.79; H, 3.84; N, 14.81.

3-(6-Bromo-3-(2-methoxybenzyl)-3H-imidazo[4,5-b]pyridin-2-yl)pyridin-2-amine (3d). Step 1: 5-Bromo-*N*-(2-methoxybenzyl)-3-nitropyridin-2-amine (**2c**) was prepared as described for **2a** using **1b** and (2-methoxyphenyl)methanamine. Step 2: **3d** was prepared from **2c** as described for **3a** using 2-aminonicotinaldehyde. Mp 179–181 °C. 1H NMR (400 MHz, DMSO- d_6) δ 8.45 (s, 2H), 8.08 (dd, $J = 4.8, 1.8$ Hz, 1H), 7.55 (dd, $J = 7.6, 1.8$ Hz, 1H), 7.25–7.16 (m, 1H), 6.97 (d, $J = 8.0$ Hz, 1H), 6.79–6.66 (m, 3H), 6.64–6.51 (m, 2H), 5.44 (s, 2H), 3.72 (s, 3H). MS m/z 410 [M + H] $^+$.

6-Bromo-3-(2-methoxybenzyl)-2-(pyridin-4-yl)-3H-imidazo[4,5-b]pyridine (3e). **3e** was prepared as described for **3a** using **2c** and isonicotinaldehyde. Mp 167–172 °C. 1H NMR (400 MHz, acetone- d_6) δ : 8.86–8.83 (dd, $J = 4.7, 1.9$ Hz, 2H), 8.52–8.39 (dd, $J = 4.6, 2.3$ Hz, 2H), 7.95–7.93 (dd, $J = 4.7, 1.9$ Hz, 2H), 7.30–7.23 (m, 1H), 7.02–6.99 (d, $J = 7.8$ Hz, 1H), 6.82–6.79 (m, 2H), 5.74 (s, 2H), 3.77 (s, 9H). MS m/z 395 [M + H] $^+$. Anal. Calcd for $C_{19}H_{15}BrN_4O \cdot 1.02TFA \cdot 0.15$ acetone: C, 49.61; H, 3.28; N, 10.77. Found: C, 49.59; H, 2.95; N, 10.76.

3-(4-(tert-Butyl)phenyl)-2-(pyridin-3-yl)-3H-imidazo[4,5-b]pyridine (3f). **3f** was prepared as described for **3a** using **2a** and nicotinaldehyde. Mp 171–175 °C. 1H NMR (400 MHz, DMSO- d_6) δ 8.69 (d, $J = 2.2$ Hz, 1H), 8.60 (dd, $J = 4.8, 1.6$ Hz, 1H), 8.34 (dd, $J = 4.7, 1.4$ Hz, 1H), 8.24 (dd, $J = 8.0, 1.4$ Hz, 1H), 7.93 (m, 1H), 7.56 (d, $J = 2.2$ Hz, 2H), 7.44 (dd, $J = 8.0, 4.8$ Hz, 1H), 7.42–7.35 (m, 3H), 1.33 (s, 9H). MS m/z 329 [M + H] $^+$. Anal. Calcd for $C_{21}H_{21}ON_4 \cdot 0.03H_2O$: C, 76.68; H, 6.15; N, 17.03. Found: C, 76.68; H, 6.25; N, 16.87.

3-(6-Bromo-3-(4-(tert-butyl)phenyl)-3H-imidazo[4,5-b]pyridin-2-yl)pyridine-2-amine (3g). Step 1: 5-Bromo-*N*-(4-(tert-butyl)phenyl)-3-nitropyridin-2-amine (**2d**) was prepared as described for **2a** using **1b**. Step 2: **3g** was prepared from **2d** as described for **3a** using 2-aminonicotinaldehyde. Mp 129–131 °C. 1H NMR (400 MHz, DMSO- d_6) δ 8.50 (d, $J = 2.1$ Hz, 1H), 8.41 (d, $J = 2.1$ Hz, 1H), 8.00 (dd, $J = 4.8, 1.9$ Hz, 1H), 7.55 (d, $J = 8.7$ Hz, 3H), 7.36 (d, $J = 8.6$ Hz, 3H), 7.23 (dd, $J = 7.7, 1.9$ Hz, 1H), 6.94 (s, 3H), 6.41 (dd, $J = 7.7, 4.8$ Hz, 1H), 1.33 (s, 9H). MS m/z 422 [M + H] $^+$.

3-(3-(3-(tert-Butyl)phenyl)-3H-imidazo[4,5-b]pyridin-2-yl)pyridin-2-amine (3h). Step 1: *N*-(3-(tert-Butyl)phenyl)-3-nitropyridin-2-amine (**2e**) was prepared as described for **2a** using 3-(tert-butyl)aniline. Step 2: **3h** was prepared from **2e** as described for **3a** using 2-aminonicotinaldehyde. Mp 198–200 °C. 1H NMR (400 MHz, DMSO- d_6) δ 8.41 (t, $J = 1.6$ Hz, 1H), 8.11 (dd, $J = 4.7, 1.6$ Hz, 1H), 8.08 (dd, $J = 12.1, 1.6$ Hz, 1H), 7.53–7.50 (m, 2H), 7.40–7.30 (m, 2H), 7.18 (d, $J = 1.6$ Hz, 1H), 7.03 (d, $J = 7.8$ Hz, 1H), 6.62 (s, 2H), 6.36–6.33 (m, 1H), 1.23 (s, 9H). MS m/z 344 [M + H] $^+$.

tert-Butyl 4-(2-(2-Aminopyridin-3-yl)-3H-imidazo[4,5-b]pyridin-3-yl)benzylcarbamate (4a). Step 1: *tert*-Butyl 4-((3-nitropyridin-2-yl)amino)benzylcarbamate (**2f**) was prepared as described for **2a** and using *tert*-butyl 4-aminobenzylcarbamate. Step 2: To a solution of **2f** (3.3 g, 9.6 mmol) in DMSO (80 mL) and methanol (14 mL) was added 2-aminonicotinaldehyde (1.3 g, 10.6 mmol) and $Na_2S_2O_4$ (85%, 4.9 g, 24 mmol). The mixture was heated at 100 °C for 15 h. After cooling to room temperature, the mixture was diluted with DCM (200 mL) and washed with H_2O and brine (200 mL). The organic phase was separated and dried over Na_2SO_4 . After filtration the solvent was removed under reduced pressure. The

residue was purified by column chromatography (0–20% methanol/DCM, silica gel) to give **4a** as a yellow solid (2.0 g, 72%). Mp 141–142 °C. 1H NMR (400 MHz, DMSO- d_6) δ 8.31 (d, $J = 4.4$ Hz, 1H), 8.19 (d, $J = 8.4$ Hz, 1H), 7.99–7.98 (m, 1H), 7.51–7.40 (m, 1H), 7.39–7.37 (m, 5H), 7.21–7.19 (m, 1H), 7.00 (bs, 2H), 6.41–6.38 (m, 1H), 4.21 (d, $J = 6.0$ Hz, 2H), 1.41 (s, 9H). MS m/z 417 [M + H] $^+$.

tert-Butyl 4-(2-(Pyridin-3-yl)-3H-imidazo[4,5-b]pyridin-3-yl)benzylcarbamate (4b). A solution of **2f** (0.5 g, 1.45 mmol), sodium dithionite (1.5 g, 8.6 mmol), and pyridine-3-carboxaldehyde (0.16 mL, 1.74 mmol) in DMSO (5 mL) and methanol (2.5 mL) was heated at 100 °C for 24 h. The mixture was cooled to room temperature and methanol removed under reduced pressure. H_2O (10 mL), tetrahydrofuran (15 mL), and saturated sodium carbonate (30 mL) were added followed by di-*tert*-butyl dicarbonate (1 g). After being stirred at room temperature for 3 h, the mixture was poured into ethyl acetate (150 mL), washed with H_2O (300 mL), and dried over anhydrous magnesium sulfate. The solids were removed by filtration, and the supernatant was evaporated to dryness under reduced pressure. The yellow oil was purified by column chromatography (70–100% ethyl acetate in hexanes, silica gel) to yield **4b** as an off-white solid (0.27 g, 46%). Mp 182–183 °C. 1H NMR (400 MHz, $CDCl_3$) δ 8.84 (d, $J = 0.8$ Hz, 1H), 8.63 (dd, $J = 4.6, 1.6$ Hz, 1H), 8.42 (dd, $J = 4.6, 1.6$ Hz, 1H), 8.18 (dd, $J = 4.6, 1.6$ Hz, 1H), 7.93 (m, 1H), 7.47–7.45 (m, 2H), 7.37–7.29 (m, 4H), 5.3 (s, 1H), 4.41 (d, $J = 6.0$ Hz, 2H), 1.48 (s, 9H). MS m/z 402 [M + H] $^+$.

tert-Butyl 4-(2-(2-Aminopyridin-3-yl)-3H-imidazo[4,5-b]pyridin-3-yl)phenylcarbamate (4c). **4c** was prepared as described for **4a** using **2h**. Mp 215–218 °C. 1H NMR (400 MHz, DMSO- d_6) δ 9.60 (s, 1H), 8.30 (dd, $J = 4.8, 1.5$ Hz, 1H), 8.17 (dd, $J = 8.0, 1.5$ Hz, 1H), 7.97 (dd, $J = 4.8, 1.8$ Hz, 1H), 7.56 (d, $J = 8.8$ Hz, 2H), 7.36 (dd, $J = 8.0, 4.8$ Hz, 1H), 7.28 (d, 2H), 7.20 (dd, $J = 7.7, 1.8$ Hz, 1H), 7.01 (s, 2H), 6.40 (dd, $J = 7.7, 4.8$ Hz, 1H), 1.47 (s, 9H). MS m/z 403 [M + H] $^+$.

3-(3-(4-(Aminomethyl)phenyl)-3H-imidazo[4,5-b]pyridin-2-yl)pyridin-2-amine Hydrochloride (5a). To a solution of **4a** (0.7 g, 1.7 mmol) in methanol (5 mL) was added HCl (4 M in dioxane, 7.2 mL, 28.8 mmol), and the mixture was stirred at room temperature for 4 h. Concentration of the solution under reduced pressure gave **5a** (0.82 g, quantitative yield) as the hydrochloric acid salt. Mp 255–257 °C. 1H NMR (400 MHz, DMSO- d_6) δ 8.44 (m, 3H), 8.30 (dd, $J = 8.0, 1.4$ Hz, 1H), 8.12 (dd, $J = 6.2, 1.6$ Hz, 1H), 7.87 (d, $J = 6.6$ Hz, 1H), 7.65 (d, $J = 8.4$ Hz, 2H), 7.57 (d, $J = 8.4$ Hz, 2H), 7.48 (dd, $J = 8.0, 4.7$ Hz, 1H), 6.85 (dd, $J = 7.1, 6.6$ Hz, 1H), 4.12 (d, $J = 5.6$ Hz, 2H), 3.81 (s, 2H). MS m/z 317 [M + H] $^+$. Anal. Calcd for $C_{18}H_{16}BrN_6 \cdot 4.6HCl \cdot 4.2H_2O \cdot 0.8Et_2O$: C, 41.12; H, 6.02; N, 13.58. Found: C, 41.13; H, 6.02; N, 13.58.

4-(2-(Pyridin-3-yl)-3H-imidazo[4,5-b]pyridin-3-yl)phenylmethanamine (5b). **5b** was prepared as described for **5a** using **4b**. Mp 265–270 °C. 1H NMR (400 MHz, DMSO- d_6) δ 8.82 (d, $J = 1.6$ Hz, 1H), 8.75 (dd, $J = 4.6, 1.6$ Hz, 1H), 8.61 (s, 3H), 8.4 (dd, $J = 4.6, 1.6$ Hz, 1H), 8.31 (dd, $J = 4.6, 1.6$ Hz, 1H), 8.13 (m, 1H), 7.71–7.65 (m, 3H), 7.57 (d, $J = 8.0$ Hz, 2H), 7.47 (dd, $J = 8.0, 4.6$ Hz, 1H), 4.13 (dd, $J = 11.4, 5.5$ Hz, 2H). MS m/z 302 [M + H] $^+$. Anal. Calcd for $C_{18}H_{16}N_6 \cdot 2.07HCl \cdot 3.14H_2O$: C, 49.89; H, 5.43; N, 16.16. Found: C, 49.90; H, 5.43; N, 15.51.

N-(4-(2-(2-Aminopyridin-3-yl)-3H-imidazo[4,5-b]pyridin-3-yl)phenyl)acetamide (5c). **5c** was prepared as described for **3a** using **2g** and 2-aminonicotinaldehyde. Mp 258–261 °C. 1H NMR (400 MHz, DMSO- d_6) δ 10.16 (s, 1H), 8.31 (dd, $J = 4.8, 1.4$ Hz, 1H), 8.18 (dd, $J = 8.0, 1.4$ Hz, 1H), 7.98 (dd, $J = 4.8, 1.8$ Hz, 1H), 7.69 (d, $J = 8.8$ Hz, 2H), 7.37 (dd, $J = 8.0, 4.8$ Hz, 1H), 7.33 (d, $J = 8.8$ Hz, 2H), 7.20 (dd, $J = 7.7, 1.8$ Hz, 1H), 7.02 (s, 2H), 6.41 (dd, $J = 7.7, 4.8$ Hz, 1H), 2.07 (s, 3H). MS m/z 345 [M + H] $^+$.

3-(3-(4-Aminophenyl)-3H-imidazo[4,5-b]pyridin-2-yl)pyridin-2-amine Hydrochloride (5d). **5d** was prepared as described for **5a** using **4c**. Mp 210–215 °C. 1H NMR (400 MHz, DMSO- d_6) δ 8.41 (dd, $J = 4.7, 1.5$ Hz, 1H), 8.28 (dd, $J = 8.1, 1.5$ Hz, 1H), 8.12 (dd, $J = 6.2, 1.6$ Hz, 1H), 7.91 (dd, $J = 7.5, 1.6$ Hz, 1H), 7.45 (dd, $J = 8.0, 4.7$ Hz, 2H), 7.31–7.19 (m, 1H), 6.89 (dd, $J = 7.5, 6.3$ Hz, 1H). MS

m/z 303 [M + H]⁺. Anal. Calcd for C₁₇H₁₄N₆·3.13HCl·0.16 dioxane: C, 49.21; H, 4.31; N, 19.52. Found: C, 49.21; H, 4.50; N, 19.53.

N-(4-(2-(2-Aminopyridin-3-yl)-3H-imidazo[4,5-b]pyridin-3-yl)phenyl)benzamide (5e). Step 1: *N*-(4-((3-Nitropyridin-2-yl)amino)phenyl)benzamide (**2i**) was prepared as described for **2a** using *N*-(4-aminophenyl)benzamide. Step 2: To a solution of **2i** (0.67 g, 0.2 mmol) in DMSO (0.7 mL) and methanol (0.7 mL) were added Na₂S₂O₄ (0.35 g, 0.4 mmol) and 2-aminonicotinaldehyde (0.29 g, 0.24 mmol). The mixture was heated at 100 °C for 24 h, cooled to room temperature, diluted with EtOAc (20 mL), and washed with H₂O (10 mL) and brine (10 mL). The organic layer was separated and concentrated. The residue was purified by column chromatography (0–20% MeOH–DCM, silica gel) to give **5e** as a light yellow solid (0.09 g, 11%). Mp 222–224 °C. ¹H NMR (400 MHz, DMSO-*d*₆) δ 10.48 (s, 1H), 8.38 (dd, *J* = 4.7, 1.4 Hz, 1H), 8.25 (dd, *J* = 8.0, 1.4 Hz, 1H), 8.05 (dd, *J* = 5.7, 1.6 Hz, 1H), 7.98–7.90 (m, 5H), 7.62 (dd, *J* = 15.3, 7.8 Hz, 2H), 7.54 (t, *J* = 7.3 Hz, 2H), 7.47–7.40 (m, 3H), 6.75–6.67 (m, 1H). MS *m/z* 407 [M + H]⁺.

Ethyl 2-(4-(2-(2-Aminopyridin-3-yl)-3H-imidazo[4,5-b]pyridin-3-yl)phenyl)acetate. (6a). Step 1: Ethyl 2-(4-((3-nitropyridin-2-yl)amino)phenyl)acetate (**2j**) was prepared as described for **2a** using ethyl 2-(4-aminophenyl)acetate and used without further purification. Step 2: To a solution of **2j** (5.5 g, 18.3 mmol) and 2-aminopyridine-3-carboxaldehyde (2.7 g, 21.9 mmol) in DMSO (60 mL) and MeOH (10 mL) was added Na₂S₂O₄ (7.9 g, 45.7 mmol). The mixture was heated at 100 °C for 24 h. EtOAc (300 mL) and H₂O (100 mL) were added, and the organic layer was separated, washed with brine (80 mL), dried over Na₂SO₄, filtered, and concentrated to dryness under reduced pressure. The residue was purified by column chromatography (EtOAc/DCM (1:1), silica gel) to give **6a** as a pale yellow solid (2.7 g, 40%). Mp 138–140 °C. ¹H NMR (400 MHz, DMSO-*d*₆) δ 8.34–8.32 (dd, *J* = 5.2 Hz, 1.6 Hz, 1H), 8.23–8.20 (dd, *J* = 8.0, 1.6 Hz, 1H), 8.01–7.99 (dd, *J* = 4.8, 2.0 Hz, 1H), 7.44–7.38 (m, 5H), 7.22–7.19 (dd, *J* = 8.4, 1.6 Hz, 1H), 6.98 (s, 2H), 6.42–6.38 (dd, *J* = 8.0, 5.2 Hz, 1H), 4.12 (q, *J* = 7.6 Hz, 2H), 3.78 (s, 2H), 1.21 (t, *J* = 6.8 Hz, 3H). MS *m/z* 374 [M + H]⁺.

Ethyl 2-(4-(2-(2-Aminopyridin-3-yl)-5-chloro-3H-imidazo[4,5-b]pyridin-3-yl)phenyl)acetate (6b). Step 1: Ethyl 2-(4-((6-chloro-3-nitropyridin-2-yl)amino)phenyl)acetate (**2k**) was prepared as described for **2a** using **1c** and ethyl 2-(4-aminophenyl)acetate and used without further purification. Step 2: **6b** was prepared from **2k** as described for **6a**. Mp 138–140 °C. ¹H NMR (400 MHz, DMSO-*d*₆) δ 8.60 (d, *J* = 8.0 Hz, 1H), 8.00–7.99 (dd, *J* = 4.8, 2.0 Hz, 1H), 7.47–7.39 (m, 5H), 7.22–7.19 (dd, *J* = 8.4, 1.6 Hz, 1H), 6.90 (s, 2H), 6.41–6.38 (dd, *J* = 8.0, 5.2 Hz, 1H), 4.12 (q, *J* = 7.6 Hz, 2H), 3.78 (s, 2H), 1.21 (t, *J* = 6.8 Hz, 3H). MS *m/z* 408 [M + H]⁺.

tert-Butyl 4-(2-(2-Aminopyridin-3-yl)-6-bromo-3H-imidazo[4,5-b]pyridine-3-yl)benzylcarbamate (6c). **6c** was prepared from **2l** as described for **6a**. Mp 176–178 °C. ¹H NMR (400 MHz, DMSO-*d*₆) δ 8.50 (d, *J* = 2.0 Hz, 1H), 8.40 (d, *J* = 2.4 Hz, 1H), 7.99 (dd, *J* = 4.7, 2.0 Hz, 1H), 7.48 (t, *J* = 5.6 Hz, 1H), 7.40–7.31 (m, 3H), 7.23 (dd, *J* = 7.8, 2.0 Hz, 1H), 6.97 (s, 2H), 6.40 (dd, *J* = 7.7, 4.4 Hz, 1H), 4.121 (d, *J* = 6.2 Hz, 2H), 1.41 (s, 9H). MS *m/z* 495 [M + H]⁺.

tert-Butyl 4-(2-(2-Aminopyridin-3-yl)-5-chloro-3H-imidazo[4,5-b]pyridin-3-yl)benzylcarbamate (6d). **6d** was prepared from **2m** as described for **6a**. Mp 235–237 °C. ¹H NMR (400 MHz, DMSO-*d*₆) δ 8.26 (d, *J* = 8.6 Hz, 1H), 7.98 (dd, *J* = 4.7, 1.9 Hz, 1H), 7.48–7.44 (m, 2H), 7.38 (s, 4H), 7.21 (dd, *J* = 7.4, 1.9 Hz, 1H), 6.92 (s, 2H), 6.39 (dd, *J* = 7.6, 4.8 Hz, 1H), 4.21 (d, *J* = 6.2 Hz, 2H), 1.41 (s, 9H). MS *m/z* 451 [M + H]⁺.

tert-Butyl 3-(2-(2-Aminopyridin-3-yl)-3H-imidazo[4,5-b]pyridine-3-yl)benzylcarbamate (6e). Step 1: *tert*-Butyl 3-((3-nitropyridin-2-yl)amino)benzylcarbamate (**2n**) was prepared as described for **2a** using *tert*-butyl 3-aminobenzylcarbamate and used without further purification. Step 2: **6e** was prepared from **2n** as described for **6a**. Mp 90–93 °C. ¹H NMR (400 MHz, DMSO-*d*₆) δ 8.30 (dd, *J* = 4.7, 1.4 Hz, 1H), 8.23–8.15 (m, 1H), 7.97 (dd, *J* = 4.8, 1.8 Hz, 1H), 7.50–7.29 (m, 5H), 7.19–7.01 (m, 4H), 6.35 (dd, *J* = 7.7, 4.8 Hz, 1H), 4.15 (d, *J* = 6.2 Hz, 2H), 1.35 (s, 9H). MS *m/z* 417 [M + H]⁺.

3-(3-(4-(Aminomethyl)phenyl)-5-chloro-3H-imidazo[4,5-b]pyridin-2-yl)pyridin-2-amine Hydrochloride (5g). **5g** was prepared from **6d** as described for **5a**. Mp 208–211 °C. ¹H NMR (400 MHz, DMSO-*d*₆) δ 8.48 (brs, 2H), 8.32 (d, *J* = 8.4 Hz, 2H), 8.15 (d, *J* = 6.2 Hz, 1H), 7.93 (d, *J* = 7.4 Hz, 1H), 7.69–7.67 (m, 2H), 7.58–7.53 (m, 3H), 6.90 (t, *J* = 7.0 Hz, 1H), 4.08 (d, *J* = 5.2 Hz, 2H). MS *m/z* 351 [M + H]⁺.

2-(4-(2-(2-Aminopyridin-3-yl)-3H-imidazo[4,5-b]pyridin-3-yl)phenyl)-*N*-phenylacetamide (7). Step 1: To a solution of **6a** (7.2 g, 19.3 mmol) in THF (40 mL) and MeOH (10 mL) was added LiOH·H₂O (0.97 g, 1.2 mmol) in H₂O (10 mL). The mixture was stirred at room temperature for 6 h. The solvent was evaporated under reduced pressure to yield lithium 2-(4-(2-(2-aminopyridin-3-yl)-3H-imidazo[4,5-b]pyridin-3-yl)phenyl)acetate (**6f**) (7.3 g) which was used in the next step without further purification. Step 2: To a solution of **6f** (3.5 g, 10.0 mmol) and aniline (1.36 mL, 14.9 mmol) in DMF (40 mL) was added HBTU (5.6 g, 14.9 mmol). The mixture was stirred at room temperature for 6 h and concentrated to half volume. DCM (300 mL) and saturated NaHCO₃ solution (80 mL) were added. The organic layer was separated and washed with brine (80 mL). After 30 min the precipitate was removed by filtration, washed with a mixture of DCM:H₂O (1:3) (20 mL) and dried to give **7** as a white solid (2.8 g, 67%). Mp 251–253 °C. ¹H NMR (400 MHz, DMSO-*d*₆) δ 10.24 (s, 1H), 8.32–8.30 (dd, *J* = 4.4, 1.2 Hz, 1H), 8.22–8.19 (dd, *J* = 8.4, 1.6 Hz, 1H), 8.01–7.99 (dd, *J* = 4.8, 1.6 Hz, 1H), 7.63–7.61 (d, *J* = 8.4 Hz, 2H), 7.49–7.47 (d, *J* = 8.4 Hz, 2H), 7.40–7.37 (m, 3H), 7.31 (t, *J* = 7.6 Hz, 2H), 7.25–7.22 (dd, *J* = 8.4, 1.6 Hz, 2H), 6.99 (s, 2H), 6.42–6.39 (dd, *J* = 7.6, 4.4 Hz, 1H), 4.12 (q, *J* = 7.6 Hz, 2H), 3.78 (s, 2H), 1.21 (t, *J* = 6.8 Hz, 3H). MS *m/z* 421 [M + H]⁺.

N-(4-(2-(2-Aminopyridin-3-yl)-3H-imidazo[4,5-b]pyridin-3-yl)benzyl)benzamide (8a). A mixture of benzoic acid (0.11 g, 0.91 mmol), DIEA (1.15 mL, 6.60 mmol), and HBTU (0.34 g, 0.91 mmol) in anhydrous DMF (2 mL) was stirred at room temperature for 5 min before **5a** (0.40 g, 0.824 mmol) was added. The mixture was stirred at room temperature for 2 h, diluted with EtOAc (20 mL), and washed with H₂O (20 mL × 3). The organic layer was concentrated to half volume and the precipitate removed by filtration and rinsed with EtOAc. Drying under vacuum yielded **8a** (0.24 g, 62%). Mp 226–228 °C. ¹H NMR (400 MHz, DMSO-*d*₆) δ 9.14 (t, *J* = 6.0 Hz, 1H), 8.31 (dd, *J* = 4.8, 1.5 Hz, 1H), 8.20 (dd, *J* = 8.0, 1.4 Hz, 1H), 7.99 (dd, *J* = 4.8, 1.8 Hz, 1H), 7.92 (dd, *J* = 5.3, 3.3 Hz, 2H), 7.60–7.34 (m, 6H), 7.24 (dd, *J* = 7.7, 1.8 Hz, 1H), 6.98 (s, 2H), 6.41 (dd, *J* = 7.6, 4.8 Hz, 1H), 4.57 (d, *J* = 6.0 Hz, 2H). MS *m/z* 421 [M + H]⁺.

N-(4-(2-(2-Aminopyridin-3-yl)-3H-imidazo[4,5-b]pyridin-3-yl)benzyl)cyclohexanecarboxamiden (8b). Cyclohexanecarboxylic acid (0.11 g, 0.82 mmol) and CDI (0.13 g, 0.82 mmol) in DMA (4 mL) were stirred for 1 h at room temperature. This mixture was added to a solution of **5a** (0.29 g, 0.81 mmol) in DMA (4 mL) and triethylamine (0.47 mL, 3.2 mmol) over 10 min. The mixture was stirred for 2 h at room temperature before the addition of H₂O (8 mL). The precipitate formed was removed by filtration, washed with H₂O and ether to yield **8b** (0.21 g, 61%). Mp 160–162 °C. ¹H NMR (400 MHz, DMSO-*d*₆) δ 8.31 (d, *J* = 3.4 Hz, 2H), 8.20 (d, *J* = 8.0 Hz, 1H), 7.99 (d, *J* = 4.2 Hz, 1H), 7.47–7.27 (m, 4H), 7.21 (d, *J* = 7.6 Hz, 1H), 6.98 (s, 2H), 6.40 (dd, *J* = 7.6, 4.9 Hz, 1H), 4.33 (d, *J* = 5.9 Hz, 2H), 2.19 (t, *J* = 11.6 Hz, 1H), 1.71 (m, 5H), 1.61–1.28 (m, 3H), 1.25–0.99 (m, 3H). MS *m/z* 427 [M + H]⁺. Anal. Calcd for C₂₅H₂₆N₆O·1.17H₂O·0.38Et₂O: C, 66.95; H, 6.81; N, 17.66. Found: C, 66.96; H, 6.56; N, 17.67.

N-(4-(2-(2-Aminopyridin-3-yl)-3H-imidazo[4,5-b]pyridin-3-yl)benzyl)-2-phenylacetamide (8c). **8c** was prepared as described for **8b** using 2-phenylacetic acid. Mp 158–160 °C. ¹H NMR (400 MHz, DMSO-*d*₆) δ 8.64 (t, *J* = 6.4 Hz, 2H), 8.31 (dd, *J* = 4.7, 1.3 Hz, 1H), 8.20 (dd, *J* = 8.0, 1.2 Hz, 1H), 8.00 (dd, *J* = 4.8, 1.8 Hz, 1H), 7.63–7.31 (m, 5H), 7.30–7.03 (m, 5H) 6.97 (s, 2H), 6.40 (dd, *J* = 7.5, 5.0 Hz, 1H), 4.36 (d, *J* = 6.0 Hz, 2H), 3.53 (s, 2H). MS *m/z* 435 [M + H]⁺. Anal. Calcd for C₂₆H₂₂N₆O·0.03EtOAc·0.32Et₂O: C, 71.41; H, 5.56; N, 18.24. Found: C, 71.41; H, 5.29; N, 18.22.

N-(4-(2-(2-Aminopyridin-3-yl)-3H-imidazo[4,5-b]pyridin-3-yl)benzyl)acetamide (8d). A solution of **5a** (0.10 g, 0.21 mmol) in

DCM (1 mL), DIPEA (0.29 mL, 1.6 mmol), and acetyl chloride 0.024 g, 0.31 mmol) was heated at 50 °C for 2 h. The mixture was diluted with EtOAc (20 mL) and washed three times with H₂O (10 mL). The organic layer was evaporated under reduced pressure and the residue purified by column chromatography (0–20% MeOH/DCM, silica gel) to yield **8d** (0.014 g, 19%). Mp 257–259 °C. ¹H NMR (400 MHz, DMSO-*d*₆) δ 8.45 (t, *J* = 6.0 Hz, 1H), 8.31 (dd, *J* = 4.6, 1.4 Hz, 1H), 8.20 (dd, *J* = 8.4, 1.6 Hz, 1H), 8.00 (dd, *J* = 4.8, 2.0 Hz, 1H), 7.4–7.37 (m, 6H), 7.22 (dd, *J* = 7.8, 1.8 Hz, 1H), 6.97 (s, 2H), 6.40 (dd, *J* = 8.0, 4.8 Hz, 1H), 4.33 (d, *J* = 6.0 Hz, 2H), 1.9 (s, 3H). MS *m/z* 359 [M + H]⁺.

N-(4-(2-(2-Aminopyridin-3-yl)-6-bromo-3H-imidazo[4,5-b]pyridin-3-yl)benzyl)benzamide (8e). Step 1: 3-(3-(4-(Aminomethyl)phenyl)-6-bromo-3H-imidazo[4,5-b]pyridin-2-yl)-pyridin-2-amine hydrochloride (**5f**) was prepared as described for **5a** from **6c**. Step 2: **5f** (4.12 g, 8.76 mmol), benzoic acid (1.49 g, 12.2 mmol), 1-ethyl-3-(3-dimethylaminopropyl)carbodiimide (5.06 g, 29.2 mmol), and DIEA (25 mL) in DCM (50 mL) were stirred at room temperature for 16 h. The mixture was diluted with DCM (10 mL) and washed with H₂O (3 × 40 mL). The organic layer was concentrated under reduced pressure to an orange oily solid (6.2 g) and purified by column chromatography (75% EtOAc/hexanes to 100% EtOAc, silica gel) to yield **8e** as an off-white solid (2.84 g, 65%). Mp 195–197 °C. ¹H NMR (400 MHz, DMSO-*d*₆) δ 9.11 (t, *J* = 5.8 Hz, 1H), 8.47 (d, *J* = 2.4 Hz, 1H), 8.36 (d, *J* = 2.4 Hz, 1H), 7.97 (dd, *J* = 5.0, 1.9 Hz, 1H), 7.88 (d, *J* = 7.1 Hz, 2H), 7.54–7.36 (m, 8H), 7.22 (dd, *J* = 7.8, 1.9 Hz, 1H), 6.92 (s, 2H), 6.39 (dd, *J* = 7.8, 5.1 Hz, 1H), 4.54 (d, *J* = 6.3 Hz, 2H). MS *m/z* 499 [M + H]⁺. Anal. Calcd for C₂₅H₁₉BrN₆O·0.07EtOAc: C, 60.06; H, 3.90; N, 16.62. Found: C, 60.03; H, 3.30; N, 16.37.

N-(3-(2-(2-Aminopyridin-3-yl)-3H-imidazo[4,5-b]pyridin-3-yl)benzyl)benzamide (8g). Step 1: **6e** was deprotected as described for **5a** from **4a** and the product used without further purification. Step 2: **8g** was prepared from the product from step 1 as described for the preparation of **8a** from **5a**. Mp 106–107 °C. ¹H NMR (400 MHz, DMSO-*d*₆) δ 9.07 (br t, *J* = 6.0 Hz, 1H), 8.32 (dd, *J* = 4.7, 1.4 Hz, 1H), 8.21 (dd, *J* = 8.0, 1.4 Hz, 1H), 7.95 (dd, *J* = 4.9, 1.8 Hz, 1H), 7.88–7.81 (m, 1H), 7.58–7.35 (m, 5H), 7.35–7.29 (m, 1H), 7.23 (dd, *J* = 7.7, 1.7 Hz, 1H), 7.18 (s, 1H), 6.37 (dd, *J* = 7.7, 4.9 Hz, 1H), 4.51 (d, *J* = 6.0 Hz, 2H). MS *m/z* 421 [M + H]⁺.

3-(3-(4-(Benzylamino)methyl)phenyl)-3H-imidazo[4,5-b]pyridin-2-yl)pyridin-2-amine (8h). To a suspension of **5a** (0.361 g, 0.72 mmol) in DCE (10 mL) and triethylamine (0.703 mL, 5.04 mmol) was added acetic acid (0.5 mL, 8.73 mmol) followed by benzaldehyde (0.07 mL, 0.66 mmol). The mixture was stirred at room temperature for 30 min before tetramethylammonium triacetoxymethylborohydride (0.28 g, 1.08 mmol) was added. After 16 h additional tetramethylammonium triacetoxymethylborohydride (0.47 g, 1.80 mmol) was added. After 4 h the mixture was diluted with saturated aqueous Na₂CO₃ (50 mL) and DCM (50 mL). The organic layer was separated, dried over sodium sulfate, filtered, and concentrated under reduced pressure. The residue was purified by column chromatography (100% DCM to 10% MeOH in DCM, silica gel) to give **8h** as a light yellow solid (0.084 g, 30%). Mp 151–152 °C. ¹H NMR (400 MHz, DMSO-*d*₆) δ 8.38–8.25 (m, 1H), 8.23–8.13 (m, 1H), 8.01–7.91 (m, 1H), 7.48 (d, *J* = 8.1 Hz, 2H), 7.43–7.26 (m, 7H), 7.26–7.14 (m, 2H), 6.99 (s, 2H), 6.37 (ddd, *J* = 7.6, 4.8, 0.7 Hz, 1H), 3.72 (d, *J* = 16.6 Hz, 4H). MS *m/z* 407 [M + H]⁺.

N-(4-(2-(2-Aminopyridin-3-yl)-6-bromo-3H-imidazo[4,5-b]pyridin-3-yl)benzyl)benzamide (9). Under a nitrogen atmosphere cyclopentylzinc bromide (0.5 M, 0.6 mL, 0.3 mmol), Pd(^tBu₃P)₂ (10.2 mg, 0.02 mmol), and potassium *tert*-butoxide (22.4 mg, 0.2 mmol) were added to a solution of **8e** (0.10 g, 0.2 mmol) in tetrahydrofuran (3 mL). The reaction mixture was degassed with nitrogen for 30 min and heated to 100 °C for 15 min in a microwave. After cooling, the mixture was filtered through Celite and diluted with DCM (5 mL), H₂O (5 mL), and EDTA (100 mg, 0.34 mmol). The organic layer was separated, washed with brine (3 mL), and dried over Na₂SO₄. The solids were removed by filtration, and the solvent was evaporated under reduced pressure. The residue was purified by column

chromatography (3–20% methanol/EtOAc, silica gel) to yield **9** as a yellow solid (0.027 g, 28%). Mp 210–211 °C. ¹H NMR (DMSO-*d*₆) 400 MHz δ 8.28 (d, *J* = 2.0 Hz, 1H), 8.05 (dd, *J* = 6.0, 2.0 Hz, 1H), 7.96 (d, *J* = 2.0 Hz, 1H), 7.82–7.84 (m, 5H), 7.34–7.37 (m, 2H), 7.09–7.12 (m, 1H), 6.62 (bs, 2H), 6.37–6.40 (m, 1H), 4.74 (d, *J* = 5.1 Hz, 2H), 3.14–3.19 (m, 1H), 2.13–2.18 (m, 2H), 1.85–1.89 (m, 8H). MS *m/z* 489 [M + H]⁺.

N-(4-(2-(2-Aminopyridin-3-yl)-6-phenyl-3H-imidazo[4,5-b]pyridin-3-yl)benzyl)benzamide (12d). **8e** (0.15 g, 0.3 mmol) and phenylboronic acid (0.073 g, 0.3 mmol) were suspended in a mixture of EtOH and toluene (1:1, 10 mL). A solution of aqueous NaHCO₃ (sat.) was added (1 mL). The mixture was degassed with nitrogen for 5 min. Tetrakis(triphenylphosphine)palladium(0) (0.02 g, 0.017 mmol) was added to the mixture and heated to 100 °C for 16 h. After cooling to room temperature, the mixture was diluted with DCM (50 mL) and H₂O (20 mL). The organic layer was separated, washed with brine (20 mL), and concentrated to 15 mL in vacuo. MeOH (2 mL) was added and the mixture purified by column chromatography (3–20% MeOH in DCM, silica gel). The solid was triturated with hot DCM (20 mL) and filtered to give **12d** as a tan solid (0.039 g, 26%). Mp 248–250 °C. ¹H NMR (400 MHz, DMSO-*d*₆) δ 9.15 (t, *J* = 6.1 Hz, 1H), 8.61 (d, *J* = 2.1 Hz, 1H), 8.46 (d, *J* = 2.0 Hz, 1H), 8.01 (dd, *J* = 4.8, 1.8 Hz, 1H), 7.97–7.87 (m, 2H), 7.85–7.71 (m, 2H), 7.64–7.35 (m, 10H), 7.27 (dd, *J* = 7.7, 1.8 Hz, 1H), 7.03 (s, 2H), 6.43 (dd, *J* = 7.7, 4.8 Hz, 1H), 4.59 (d, *J* = 6.0 Hz, 2H). MS *m/z* 497 [M + H]⁺.

Ethyl 2-(4-(5-(3-Acetamidophenyl)-2-(2-aminopyridin-3-yl)-3H-imidazo[4,5-b]pyridin-3-yl)phenyl)acetate (10a). **10a** was prepared from **6b** as described for **12d** using 3-acetamidophenylboronic acid. Mp 93–95 °C. ¹H NMR (400 MHz, DMSO-*d*₆) δ 10.08 (s, 1H), 8.29–8.27 (d, *J* = 8.4 Hz, 1H), 8.10 (s, 1H), 8.00 (dd, *J* = 4.4, 1.6 Hz, 1H), 7.85 (d, *J* = 8.4 Hz, 1H), 7.11–7.65 (dd, *J* = 18.0, 6.8 Hz, 2H), 7.45 (s, 4H), 7.38 (t, *J* = 8.0 Hz, 1H), 7.19–7.17 (dd, *J* = 8.0, 2.0 Hz, 1H), 6.92 (s, 2H), 6.42–6.38 (dd, *J* = 8.0, 4.8 Hz, 1H), 4.13 (q, *J* = 7.2 Hz, 2H), 3.79 (s, 2H), 2.06 (s, 3H), 1.21 (t, *J* = 6.8 Hz, 3H). MS *m/z* 507 [M + H]⁺.

2-(4-(5-(3-Acetamidophenyl)-2-(2-aminopyridin-3-yl)-3H-imidazo[4,5-b]pyridin-3-yl)phenyl)-*N*-phenylacetamide (12a). Step 1: To a solution of **10a** (0.50 g, 0.99 mmol) in THF (6 mL) and MeOH (2 mL) was added a solution of LiOH·H₂O (0.046 g, 1.08 mmol) in H₂O (2 mL). The mixture was stirred at room temperature for 6 h. The solvent was removed under reduced pressure to give **6g** (0.55 g) which was used without further purification. Step 2: To a solution of lithium 2-(4-(5-(3-acetamidophenyl)-2-(2-aminopyridin-3-yl)-3H-imidazo[4,5-b]pyridin-3-yl)phenyl)acetate (**6g**) (0.1 g, 0.207 mmol) and aniline (31 μL, 0.331 mmol) in DMF (1 mL) was added HBTU (0.14 g, 0.372 mmol). The mixture was stirred at room temperature for 6 h. The solvent was removed under reduced pressure and the residue purified by preparative HPLC (H₂O, 0.05 M TFA/ACN, 0.05 M TFA, 0–100% ACN) to give **12a** as a yellow solid (22 mg, 19%). Mp 166–168 °C. ¹H NMR (400 MHz, DMSO-*d*₆) δ 10.25 (s, 1H), 10.03 (s, 1H), 8.33 (d, *J* = 8.8 Hz, 1H), 8.12 (s, 1H), 8.06–8.04 (dd, *J* = 5.6, 1.6 Hz, 1H), 7.71–7.61 (m, 5H), 7.51 (s, 4H), 7.39 (t, *J* = 8.0 Hz, 1H), 7.33 (t, *J* = 8.0 Hz, 2H), 7.06 (t, *J* = 7.2 Hz, 1H), 6.72 (t, *J* = 6.0 Hz, 1H), 3.77 (s, 2H), 2.04 (s, 3H). MS *m/z* 554 [M + H]⁺. Anal. Calcd for C₃₃H₂₇N₇O₂·1.82TFA: C, 57.82; H, 3.82; N, 12.88. Found: C, 57.84; H, 3.93; N, 12.93.

Ethyl 2-(4-(2-(2-Aminopyridin-3-yl)-5-(pyridin-3-yl)-3H-imidazo[4,5-b]pyridin-3-yl)phenyl)acetate (10b). **10b** was prepared from **6b** as described for **12d** using 3-pyridylboronic acid. Mp 155–157 °C. ¹H NMR (400 MHz, DMSO-*d*₆) δ 9.24 (m, 1H), 8.60–8.58 (dd, *J* = 4.8, 1.2 Hz, 1H), 8.38 (d, *J* = 8.4 Hz, 1H), 8.32 (d, *J* = 8.0 Hz, 1H), 8.08 (d, *J* = 8.4 Hz, 1H), 8.01 (dd, *J* = 5.2, 2.0 Hz, 1H), 7.52–7.44 (m, 5H), 7.22–7.20 (dd, *J* = 7.6, 2.0 Hz, 1H), 6.99 (s, 2H), 6.43–6.39 (dd, *J* = 6.8, 4.4 Hz, 1H), 4.13 (q, *J* = 7.2 Hz, 2H), 3.80 (s, 2H), 1.21 (t, *J* = 6.8 Hz, 3H). MS *m/z* 451 [M + H]⁺.

***tert*-Butyl 4-(2-(2-Aminopyridin-3-yl)-6-(pyridin-3-yl)-3H-imidazo[4,5-b]pyridin-3-yl)benzylcarbamate (10c).** **10c** was prepared from **6c** as described for **12d** using 3-pyridylboronic acid. Mp 95–100 °C. ¹H NMR (400 MHz, DMSO-*d*₆) δ 8.98 (d, *J* = 1.9 Hz, 1H), 8.64 (d, *J* = 2.0 Hz, 1H), 8.59 (dd, *J* = 4.7, 1.6 Hz, 1H), 8.54

(d, $J = 2.0$ Hz, 1H), 8.20 (m, 1H), 7.98 (m, 1H), 7.52 (m, 2H), 7.48–7.34 (m, 4H), 7.23 (m, 1H), 7.01 (s, br, 2H), 6.38 (m, 1H), 4.19 (m, 2H), 1.38 (s, 9H). MS m/z 494 [M + H]⁺.

tert-Butyl 4-(2-(2-Aminopyridin-3-yl)-5-phenyl-3H-imidazo[4,5-*b*]pyridin-3-yl)benzylcarbamate (10e). 10e was prepared from 6d as described for 12d. Mp 109–112 °C. ¹H NMR (400 MHz, DMSO-*d*₆) δ 8.24 (d, $J = 8.4$ Hz, 1H), 8.02–7.96 (m, 4H), 7.48–7.37 (m, 8H), 7.19 (d, $J = 8.0$ Hz, 1H), 6.99 (bs, 2H), 6.38 (m, 1H), 4.22 (d, $J = 5.6$ Hz, 2H), 1.39 (s, 9H). MS m/z 493 [M + H]⁺.

3-(3-(4-(Aminomethyl)phenyl)-6-(pyridin-3-yl)-3H-imidazo[4,5-*b*]pyridin-2-yl)pyridin-2-amine Hydrochloride (11a). 11a was prepared from 10c as described for 5a. Mp 223–225 °C. ¹H NMR (400 MHz, MeOH-*d*₄) δ 9.38 (d, $J = 2.0$ Hz, 1H), 9.11 (d, $J = 2.0$ Hz, 1H), 8.95–8.93 (m, 1H), 8.89 (d, $J = 2.0$ Hz, 1H), 8.78 (m, 1H), 8.83–8.25 (m, 1H), 8.06–8.04 (m, 1H), 7.88–7.86 (m, 1H), 7.77–7.66 (m, 4H), 6.86–6.83 (m, 1H), 4.23 (m, 2H). MS m/z 394 [M + H]⁺.

N-(3-(3-(4-(Aminomethyl)phenyl)-2-(2-aminopyridin-3-yl)-3H-imidazo[4,5-*b*]pyridin-5-yl)phenyl)acetamide Hydrochloride (11b). Step 1: *tert*-Butyl 4-(5-(3-acetamidophenyl)-2-(2-aminopyridin-3-yl)-3H-imidazo[4,5-*b*]pyridin-3-yl)benzylcarbamate (10d) was prepared from 6d as described for 12d using 3-acetamidophenylboronic acid. Step 2: 10d (0.23 g, 0.42 mmol) was suspended in EtOAc (5 mL) and hydrochloric acid in dioxane (4M, 10 mL) added. The mixture was stirred at 56 °C for 4 h. After the mixture was cooled to room temperature, the precipitate was collected by filtration to give 11b hydrochloride salt as a yellow solid (0.24 g, 100%). Mp 245–248 °C. ¹H NMR (400 MHz, DMSO-*d*₆) δ 10.16 (s, 1H), 8.47 (s, 3H), 8.35 (d, $J = 8.4$ Hz, 2H), 8.17 (s, 1H), 8.12 (d, $J = 6.2$ Hz, 1H), 7.89 (d, $J = 8.2$ Hz, 2H), 7.67–7.60 (m, 5H), 7.37 (t, $J = 8.0$ Hz, 1H), 6.88–6.85 (m, 1H), 4.10 (m, 2H), 2.04 (s, 3H). MS m/z 450 [M + H]⁺.

3-(3-(4-(Aminomethyl)phenyl)-5-phenyl-3H-imidazo[4,5-*b*]pyridin-2-yl)pyridin-2-amine Hydrochloride (11c). 11c was prepared from 10e as described for 11b, step 2. Mp 215–218 °C. ¹H NMR (400 MHz, DMSO-*d*₆) δ 8.52 (bs, 5H), 8.35 (d, $J = 8.4$ Hz, 1H), 8.13 (d, $J = 6.0$ Hz, 1H), 8.04 (m, 3H), 7.89 (m, 1H), 7.65 (dd, $J = 8.4, 1.6$ Hz, 4H), 7.48–7.38 (m, 3H), 6.89 (m, 1H), 4.11 (d, $J = 5.6$ Hz, 2H). MS m/z 393 [M + H]⁺.

2-(4-(5-(3-Acetamidophenyl)-2-(2-aminopyridin-3-yl)-3H-imidazo[4,5-*b*]pyridin-3-yl)phenyl)-N-(3-fluorophenyl)acetamide (12b). 12b was prepared as described for 12a using 3-fluoroaniline. Mp 150–152 °C. ¹H NMR (400 MHz, DMSO-*d*₆) δ 10.49 (s, 1H), 10.08 (s, 1H), 8.33 (d, $J = 8.4$ Hz, 1H), 8.13 (s, 1H), 8.06 (dd, $J = 4.8$ Hz, 1.6 Hz, 1H), 7.90 (d, $J = 8.4$ Hz, 1H), 7.71–7.61 (m, 4H), 7.52 (s, 4H), 7.41–7.33 (m, 3H), 6.89 (t, $J = 8.4$ Hz, 1H), 6.74 (t, $J = 7.2$ Hz, 1H), 3.79 (s, 2H), 2.04 (s, 3H). MS m/z 572 [M + H]⁺. Anal. Calcd for C₃₃H₂₆FN₇O₂·1.6TFA·0.47ACN: C, 57.68; H, 3.78; N, 12.88. Found: C, 57.70; H, 3.58; N, 13.53.

2-(4-(2-(2-Aminopyridin-3-yl)-5-(pyridin-3-yl)-3H-imidazo[4,5-*b*]pyridin-3-yl)phenyl)-N-phenylacetamide (12c). Step 1: Lithium 2-(4-(2-(2-aminopyridin-3-yl)-5-(pyridin-3-yl)-3H-imidazo[4,5-*b*]pyridin-3-yl)phenyl)acetate (6h) was prepared from 10b as described for 6g and used without further purification. Step 2: 12c was prepared from 6h as described for 12a and obtained as a yellow solid. Mp 162–164 °C. ¹H NMR (400 MHz, DMSO-*d*₆) δ 10.28 (s, 1H), 9.33 (s, 1H), 8.72 (d, $J = 4.0$ Hz, 1H), 8.63 (d, $J = 8.0$ Hz, 1H), 8.43 (d, $J = 8.4$ Hz, 1H), 8.19 (d, $J = 8.0$ Hz, 1H), 8.13–8.09 (dd, $J = 6.4, 2.0$ Hz, 1H), 7.81 (d, $J = 7.6$ Hz, 1H), 7.72 (dd, $J = 8.4, 5.2$ Hz, 1H), 7.62 (d, $J = 8.0$ Hz, 1H), 7.57–7.54 (m, 4H), 7.33 (t, $J = 6.0$ Hz, 2H), 7.06 (t, $J = 7.6$ Hz, 1H), 6.82 (t, $J = 6.8$ Hz, 1H), 3.78 (s, 2H). MS m/z 498 [M + H]⁺. Anal. Calcd for C₃₀H₂₃N₇O·3.26TFA: C, 50.46; H, 3.04; N, 11.28. Found: C, 50.47; H, 2.97; N, 11.25.

N-(4-(2-(2-Aminopyridin-3-yl)-6-(pyridin-3-yl)-3H-imidazo[4,5-*b*]pyridin-3-yl)benzyl)benzamide (12e). 12e was prepared from 11a as described for 8b using benzoic acid. Mp 257–260 °C. ¹H NMR (400 MHz, DMSO-*d*₆) δ 9.15 (t, $J = 5.6$ Hz, 1H), 9.01–9.00 (m, 1H), 8.67–8.66 (m, 1H), 8.63–8.62 (m, 1H), 8.58–8.57 (m, 1H), 8.22–8.19 (m, 1H), 8.02–8.00 (m, 1H), 7.95–7.92 (m, 2H), 7.57–7.45 (m, 8H), 7.29–7.27 (m, 1H), 7.03 (s, br, 2H), 6.45–6.42 (m, 1H), 4.59–4.58 (m, 2H). MS m/z 497 [M]⁺.

N-(4-(2-(2-Aminopyridin-3-yl)-5-(pyridin-3-yl)-3H-imidazo[4,5-*b*]pyridin-3-yl)benzyl)benzamide (12f). Step 1: To a solution of 5g (8.9 g, 25.5 mmol) in H₂O (50 mL) was added NaOH (1.51 g, 38.25 mmol) and benzoyl chloride (5.35 g, 38.25 mmol). The mixture was stirred at room temperature for 18 h. The precipitate was removed by filtration and washed with H₂O and ether to yield *N*-(4-(2-(2-aminopyridin-3-yl)-5-chloro-3H-imidazo[4,5-*b*]pyridin-3-yl)benzyl)benzamide (8f) (2.9 g, 84%) which was used without further purification. Step 2: 12f was prepared from 8f as described for 12d using 3-pyridylboronic acid. Mp 253–256 °C. ¹H NMR (400 MHz, DMSO-*d*₆) δ 9.23 (s, 1H), 9.16 (t, $J = 5.8$ Hz, 1H), 8.58 (d, $J = 7.1$ Hz, 1H), 8.37 (d, $J = 8.2$ Hz, 1H), 8.31 (d, $J = 8.2$ Hz, 1H), 8.08 (d, $J = 8.6$ Hz, 1H), 7.95 (m, 1H), 7.93 (d, $J = 8.6$ Hz, 1H), 7.48–7.55 (m, 6H), 7.24 (d, $J = 7.8$ Hz, 1H), 6.97 (s, 2H), 6.42 (m, 1H), 4.62 (d, $J = 6.2$ Hz, 2H). MS m/z 498 [M + H]⁺. Anal. Calcd for C₃₀H₂₃N₇O·0.17EtOAc: C, 71.90; H, 4.79; N, 19.13. Found: C, 71.16; H, 4.67; N, 19.12.

N-(4-(2-(2-Aminopyridin-3-yl)-6-(pyridin-3-yl)-3H-imidazo[4,5-*b*]pyridin-3-yl)benzyl)-3-fluorobenzamide (12g). 12g was prepared from 11a as described for 8b using 3-fluorobenzoic acid. Mp 258–260 °C. ¹H NMR (400 MHz, DMSO-*d*₆) δ 9.25 (t, $J = 6.0$ Hz, 1H), 8.01 (s, 1H), 9.01 (d, $J = 1.6$ Hz, 1H), 8.51 (d, $J = 3.2$ Hz, 1H), 8.58 (d, $J = 2.0$ Hz, 1H), 8.20 (d, $J = 8.4$ Hz, 1H), 8.08 (d, $J = 3.2$ Hz, 1H), 7.78 (d, $J = 7.6$ Hz, 1H), 7.72 (d, $J = 10.4$ Hz, 1H), 7.56–7.41 (m, 6H), 7.27 (d, $J = 8.0$ Hz, 1H), 7.02 (s, 2H), 6.43 (t, $J = 6.8$ Hz, 2H), 4.59 (s, 2H). MS m/z 516 [M + H]⁺. Anal. Calcd for C₃₀H₂₂N₇O·0.1H₂O·0.09DMA: C, 69.43; H, 4.42; N, 18.91. Found: C, 69.37; H, 4.37; N, 19.04.

N-(4-(5-(3-Acetamidophenyl)-2-(2-aminopyridin-3-yl)-3H-imidazo[4,5-*b*]pyridin-3-yl)benzyl)benzamide (12h). 12h was prepared from 11b as described for 8b using benzoic acid. Mp 205–208 °C. ¹H NMR (400 MHz, DMSO-*d*₆) δ 10.04 (s, 1H), 9.13 (t, $J = 6.0$ Hz, 1H), 8.25 (d, $J = 8.4$ Hz, 1H), 8.06 (s, 1H), 7.98–7.96 (m, 1H), 7.91 (d, $J = 7.2$ Hz, 2H), 7.82 (d, $J = 8.0$ Hz, 1H), 7.68 (d, $J = 8.8$ Hz, 1H), 7.63 (d, $J = 8.0$ Hz, 1H), 7.55–7.43 (m, 6H), 7.35 (t, $J = 8.0$ Hz, 1H), 7.18 (d, $J = 7.6$ Hz, 1H), 6.87 (s, 2H), 6.39 (dd, $J = 7.6, 4.8$ Hz, 1H), 4.58 (d, $J = 6.0$ Hz, 2H), 2.02 (s, 3H). MS m/z 554 [M + H]⁺.

N-(4-(2-(2-Aminopyridin-3-yl)-5-phenyl-3H-imidazo[4,5-*b*]pyridin-3-yl)benzyl)benzamide (12i). 12i was prepared from 11c as described for 8b using benzoic acid. Mp 237–240 °C. ¹H NMR (400 MHz, DMSO-*d*₆) δ 9.13 (t, $J = 8.4$ Hz, 1H), 8.23 (d, $J = 8.4$ Hz, 1H), 8.00–7.90 (m, 6H), 7.52–7.36 (m, 10H), 7.18 (d, $J = 7.6$ Hz, 2H), 6.92 (s, 2H), 6.39 (dd, $J = 4.8, 2.8$ Hz, 1H), 4.58 (d, $J = 6.0$ Hz, 2H). MS m/z 497 [M + H]⁺.

N-(4-(5-(3-Acetamidophenyl)-2-(2-aminopyridin-3-yl)-3H-imidazo[4,5-*b*]pyridin-3-yl)benzyl)-3-fluorobenzamide (12j). 12j was prepared from 11b as described for 8b using 3-fluorobenzoic acid. Mp 174–187 °C. ¹H NMR (400 MHz, DMSO-*d*₆) δ 10.03 (s, 1H), 9.22 (t, $J = 6.0$ Hz, 1H), 8.24 (d, $J = 8.4$ Hz, 1H), 8.06 (s, 1H), 7.97 (dd, $J = 4.8, 1.6$ Hz, 1H), 7.82 (d, $J = 8.8$ Hz, 1H), 7.77 (d, $J = 8.0$ Hz, 1H), 7.72–7.66 (m, 2H), 7.62 (d, $J = 8.4$ Hz, 1H), 7.55–7.51 (m, 1H), 7.45 (s, 3H), 7.41–7.32 (m, 2H), 7.18 (dd, $J = 7.6, 1.6$ Hz, 1H), 6.86 (br, 2H), 6.38 (dd, $J = 8.0, 4.8$ Hz, 1H), 4.58 (d, $J = 6.0$ Hz, 2H), 2.01 (s, 3H). MS m/z 572 [M + H]⁺. Anal. Calcd for C₃₃H₂₆FN₇O₂·1.4HCl·0.1 dioxane·0.15Et₂O: C, 63.55; H, 4.66; N, 15.26. Found: C, 63.91; H, 4.36; N, 15.38.

tert-Butyl 4-(2-(2-Aminopyridin-3-yl)-5-(pyridin-3-yl)-3H-imidazo[4,5-*b*]pyridin-3-yl)benzylcarbamate (10f). 10f was prepared from 6d as described for 12d using 3-pyridylboronic acid. Mp 223–225 °C. ¹H NMR (400 MHz, DMSO-*d*₆) δ 9.23 (d, $J = 1.7$ Hz, 1H), 8.59 (dd, $J = 4.7, 1.5$ Hz, 1H), 8.41–8.34 (m, 1H), 8.32 (d, $J = 8.3$ Hz, 1H), 8.08 (d, $J = 8.4$ Hz, 1H), 8.01 (dd, $J = 4.8, 1.8$ Hz, 1H), 7.52–7.37 (m, 5H), 7.22 (dd, $J = 7.7, 1.8$ Hz, 1H), 7.00 (s, 2H), 6.42 (dd, $J = 7.6, 4.9$ Hz, 1H), 4.24 (d, $J = 6.1$ Hz, 2H), 1.41 (s, 9H). MS m/z 494 [M + H]⁺.

N-(4-(2-(2-Aminopyridin-3-yl)-5-(pyridin-3-yl)-3H-imidazo[4,5-*b*]pyridin-3-yl)benzyl)-3-fluorobenzamide (12k). Step 1: 3-(3-(4-(Aminomethyl)phenyl)-5-(pyridin-3-yl)-3H-imidazo[4,5-*b*]pyridin-2-yl)pyridin-2-amine (11d) was prepared as described for 5a

from **10f** and was used without further purification. Step 2: **12k** was prepared from **11d** as described for **8b** using 3-fluorobenzoic acid. Mp 236–234 °C. ¹H NMR (400 MHz, DMSO-*d*₆) δ 9.26 (t, *J* = 6.0 Hz, 1H), 9.23 (d, *J* = 1.7 Hz, 1H), 8.59 (dd, *J* = 4.7, 1.6 Hz, 1H), 8.44–8.34 (m, 1H), 8.32 (d, *J* = 8.3 Hz, 1H), 8.07 (d, *J* = 8.4 Hz, 1H), 8.01 (dd, *J* = 4.8, 1.9 Hz, 1H), 7.85–7.77 (m, 1H), 7.77–7.69 (m, 1H), 7.62–7.52 (m, 1H), 7.52–7.46 (m, 5H), 7.46–7.37 (m, 1H), 7.24 (dd, *J* = 7.7, 1.8 Hz, 1H), 6.97 (s, 2H), 6.43 (dd, *J* = 7.7, 4.8 Hz, 1H), 4.62 (d, *J* = 6.0 Hz, 2H). MS *m/z* 516 [M + H]⁺.

Protein Expression and Purification. Full length Akt isoform constructs (Akt1 (2–480), Akt2 (2–481), and Akt3 (2–479)) and ΔPH-Akt1 (144–480) were expressed using a baculovirus vector in Sf9 cells. The frozen cell pellets were thawed and resuspended in lysis buffer containing 25 mM Tris, pH 8.0, 100 mM NaCl, 25 mM imidazole, 10% glycerol, protease inhibitors (Sigma no. S8820). Cells were lysed by sonication. The lysate was centrifuged, and the clarified supernatant was loaded onto a Ni-NTA affinity column. Following the washing with buffer containing 25 mM Tris, pH 8.0, 500 mM NaCl, and 25 mM imidazole, the protein was eluted in buffer containing 25 mM Tris, 100 mM NaCl, and 400 mM imidazole, pH 8.0. The protein was concentrated and purified on a Superdex 200 gel filtration column. The concentrated protein (10 mg/mL) was stored in buffer containing 25 mM Tris, pH 8.0, 100 mM NaCl, and 10% glycerol at –80 °C.

Protein Characterization (Akt1, Akt2, and Akt3). The phosphorylation state of Thr308 and Ser473 in Akt1 (1–480) was analyzed as described below. Proteins were subjected to a solution-phase digest, and the phosphorylation state of the peptides was determined by LC/MS and LC/MS/MS analysis. Protein (50 μg) was diluted in 50 mM ammonium bicarbonate buffer, pH 8, containing 5 mM DTT, 3 M urea, 5% acetonitrile, and endoprotease (trypsin, 1:20 w/w or GluC, 1:10 w/w ratio), and digested overnight. The digest was separated on a BEH C18 column (1.0 mm × 50 mm, 1.7 μm) equilibrated at 40 °C and mass-analyzed on a QTOF mass spectrometer. The elution was performed using a water/acetonitrile gradient with 0.1% formic acid modifier, starting from 2% and reaching 40% acetonitrile in 14 min, followed by 40–50% acetonitrile from 14 to 16 min, 50–80% acetonitrile from 16 to 18 min, held at 80% for 2 min, and re-equilibrated at 2% acetonitrile for another 3 min. Mass spectra of peptides were deconvoluted by the MaxEnt3 software package (Masslynx, Waters). For the inactive Akt proteins, no phosphorylation was detected on the Thr308/Thr309/Thr305 site, and less than 10% of the Ser473/Ser474/Ser472 was detected as phosphorylated (in Akt1, Akt2, and Akt3, respectively). Following activation with PDK1 and MAPKAP2 in the presence of lipids, MS analysis identified 60% of Thr308 and 80% of Ser473 as phosphorylated.

High Throughput Binding Screen by Indirect Affinity Mass Spectrometry (IA-MS) (Mixed Pool). The compound library was plated into 96-well plates as mixtures of 20 compounds per well in DMSO. Test compounds in DMSO were mixed with buffer consisting of 25 mM Tris-HCl (pH 7.5), 100 mM NaCl, and 0.1% 2-β-mercaptoethanol and incubated with inactive full length Akt1 (1–480) for 30 min at room temperature. The final binding mixture (25 μL volume) contained 10 μM Akt1 (1–480) protein, compound pool (10 μM each), and a 4% final DMSO concentration. Protein-bound inhibitors were separated from the unbound inhibitors by fast centrifugation at 4 °C through a size exclusion gel in a 96-well plate format. Controls that contained the compound pool (10 μM each) in buffer were used to verify that no inhibitor passed through the gel in the absence of protein carrier. The eluent from the size exclusion column (~25 μL) was mixed with 30 μL of an internal standard in DMSO/H₂O (1:1) and analyzed for the presence of the small molecular weight inhibitor by LC/MS. Test samples were injected onto the Acquity UPLC instrument equipped with a BEH C18 column (1.0 mm × 50 mm, 1.7 μm) and separated at 0.1 mL/min using a water/acetonitrile gradient with 0.1% formic acid modifier, starting at 10% and reaching 90% acetonitrile in 5 min, held at 90% for 1 min, and re-equilibrating at 10% acetonitrile for another 3 min. UPLC flow was directed to a QTOF mass spectrometer (Waters) equipped with an ESI probe, which was operated in the full scan monitoring mode

with the following parameters: capillary voltage 3.5 V, cone voltage 40 V, source temperature 120 °C, desolvation temperature 200 °C. Binders were identified by the detection of their molecular weight at the appropriate retention time compared with the mixtures of compound standards dissolved in DMSO and analyzed with the same analytical method.

Thermal Shift Binding Assay (Akt1 (1–480), Akt2 (1–481), and Akt3 (1–479)). The binding affinities of test compounds to the full length inactive Akt isoforms were assessed by a thermal shift binding assay. Aliquots of compounds in DMSO (1 μL at 375 μM) were placed in a V-bottom 96-well PCR plate and incubated for 30 min with 24 μL of the protein (1.5 μM) in 25 mM Tris buffer, pH 7.5, 100 mM NaCl, 0.1% 2-mercaptoethanol, premixed with environmentally sensitive fluorescent dye Sypro Orange (12.5X). The plates were centrifuged for 3 min at 2000 rpm and 25 °C before analysis on an IQ5 real time PCR machine. The thermal stability of the protein–ligand complex was monitored by changes in Sypro Orange fluorescence while subjecting the binding mixture to a temperature gradient (30 to 75 at 1 °C/min heating rate). Shifts in the protein melting temperature (Δ*T*_m) greater than 0.6 °C compared to the protein alone were indicative of inhibitor binding. The reported thermal shift data are a geometric mean of at least two measurements with typical STD of <10%.

Tryptophan Fluorescence Quench Assay. Binding of AMP-PNP and A674563 to Akt1 constructs (Akt1 (1–480) and Akt1 (144–480)) was detected by measuring the intrinsic tryptophan fluorescence. The Akt1 proteins (2 μM) were titrated with increasing concentrations of AMP-PNP or A674563. The change in intrinsic emission was measured on a Tecan microplate reader at an excitation wavelength of 295 nm and emission wavelength of 345 nm. The binding measurements were performed in a buffer solution containing 25 mM Tris, pH 7.5, 0.1 M NaCl, and 2% DMSO. The magnitude of increase in tryptophan fluorescence (Δ*F*) was calculated as Δ*F* = *F* – *F*₀, where *F* and *F*₀ are the emission intensities in the presence and absence of ligand, respectively. Dissociation constants (*K*_d) were obtained from a fit to the hyperbolic binding equation, Δ*F*/*F*₀ = *F*_{max}[L]/([L] + *K*_d), where *F*_{max} corresponds to the fluorescence intensity at saturation.

Surface Plasmon Resonance (SPR). SPR measurements were performed on a Reichert SR7500DC SPR system (Reichert Technologies, Depew, NY). Unphosphorylated Akt1 (1–480) was exchanged into sodium acetate buffer (10 mM, pH 5.2) and immobilized onto a Reichert CMD 500k chip using standard amine coupling methodology. Specifically, a solution containing 40 mg of EDC (Sigma) and 10 mg of NHS (Sigma) dissolved in 0.9 mL of doubly distilled H₂O was injected over the surface for 7 min. A 182 μg/mL solution of Akt1 (1–480) in 10 mM sodium acetate buffer with 1 mM DTT was subsequently injected over the sensor surface for about 10 min, achieving an immobilization response level of 8400 μRIU. Lastly, the surface was deactivated/blocked with an injection of 1 M ethanolamine (Sigma), pH 8.5, with 1 mM DTT for 10 min. The running buffer for immobilization was 25 mM HEPES, pH 7.4, 150 mM NaCl, 0.05% Tween 20, and 1 mM DTT. Kinetic analysis was performed at 25 °C in 25 mM Tris-HCl, pH 7.5, 100 mM NaCl, 1 mM MgCl₂, 5 mM DTT, and 5% DMSO. Test compound was prepared in the buffer used for kinetic analysis at 31.25, 62.5, 125, and 500 nM and injected over the sample and reference flow cells at 50 μL/min. The association and dissociation phases were each monitored for 3 min, and the test compound concentrations were injected from low to high without regeneration (kinetic titration approach). Data were fit to a 1:1 kinetic titration model.

Lipid Vesicles Preparation. Lipid vesicles were prepared from PtdIns(3,4,5)P₃, dipalmitoyl, and a synthetic phospholipid blend of DOPS/DOPC. A 1.0 mg/mL solution of PtdIns(3,4,5)P₃ and a 16.7 mg/mL suspension of DOPS/DOPC in 10 mM Hepes, pH 7.4, were prepared immediately before use. The DOPS/DOPC suspension (800 μL) and the PtdIns(3,4,5)P₃ solution (964 μL) were mixed and then diluted in 18.2 mL of 10 mM Hepes, pH 7.4, and mixed well. This mixture, (400 μM DOPS/400 μM DOPC/40 μM PtdIns(3,4,5)P₃),

was sonicated on ice for 30 s at 75% power until the mixture was clarified. Aliquots were prepared and frozen at -80°C until use.

Akt1 (1–480), Akt2 (1–481), and Akt3 (1–479) α Screen Assays. Akt activity was assayed using a GSK3-derived biotinylated peptide substrate, crosstide (biotin-GRPRTSSFAEG), and the AlphaScreen (amplified luminescent proximity homogeneous assay) technology. Test compounds and controls were prepared in 10% DMSO at 10-fold the desired final concentration and added to each well of a reaction plate (Corning 96-well half-area solid white nonbinding surface plate) in a volume of $2.5\ \mu\text{L}$. Full-length unphosphorylated Akt was diluted in assay buffer (50 mM Tris, pH 8.0, 0.02 mg/mL BSA, 10 mM MgCl_2 , 1 mM EGTA, 10% glycerol, 0.2 mM Na_3VO_4 , 1 mM DTT, 0.1 mM β -glycerophosphate, and 0.2 mM NaF) and added to each well in a volume of $17.5\ \mu\text{L}$ for a final concentration in the $25\ \mu\text{L}$ mixture of 8 nM (Akt1), 63 nM (Akt2), or 13 nM (Akt3). After a 20 min preincubation at room temperature, the kinase reaction was initiated by the addition of $5\ \mu\text{L}$ of the activation mixture diluted in assay buffer containing biotinylated crosstide, PDK1, MAPKAPK2, DOPS/DOPC, PtdIns(3,4,5)P3, and ATP for final concentrations of 60 nM biotinylated crosstide, 0.1 nM (Akt1, Akt3) or 0.3 nM (Akt2) PDK1, 0.7 nM (Akt1), 1.3 nM (Akt2), or 0.4 nM (Akt3) MAPKAPK2, $5.5\ \mu\text{M}$ DOPS, $5.5\ \mu\text{M}$ DOPC, $0.5\ \mu\text{M}$ PtdIns(3,4,5)P3, and $50\ \mu\text{M}$ (Akt1, Akt2) or $18\ \mu\text{M}$ (Akt3) ATP. The plates were incubated for 30 min at room temperature. The reaction was stopped in the dark by the addition of $10\ \mu\text{L}$ of stop/detection mixture prepared in the assay buffer containing EDTA, AlphaScreen streptavidin donor and protein A acceptor beads, and phospho-AKT substrate antibody for final concentrations of 10 mM EDTA, 500 ng/well of both AlphaScreen streptavidin donor beads and protein A acceptor beads, and phospho-AKT substrate antibody at a final dilution of 1:350. Assay plates were incubated for 90 min at room temperature in the dark, and the plates were read on a Perkin-Elmer Envision multilabel plate reader (excitation wavelength of 640 nm, emission wavelength of 570 nm). All IC_{50} values reported are the geometric mean of at least $n = 2$ determinations.

Akt1 (104–480). Reactions with Akt1 (Carna 01-101) enzyme in the activated form were performed as above in the AlphaScreen format with the following modifications. PDK1, MAPKAPK2, and the lipid vesicle mixture were omitted from the reaction. Active Akt1 was added for a final reaction concentration of 0.1 nM.

MAPKAPK2 Assay. MAPKAPK2 activity was assayed using the CisBio KinEASE HTRF assay technology. Test compounds and control (staurosporine) were prepared in 10% DMSO at 10-fold the desired final concentration and added to each well of a reaction plate (Corning 96-well half-area solid black nonbinding surface plate) in a volume of $2.5\ \mu\text{L}$. MAPKAPK2 was diluted into assay buffer (50 mM Tris, pH 8.0, 0.02 mg/mL BSA, 10 mM MgCl_2 , 1 mM EGTA, 10% glycerol, 0.1 mM Na_3VO_4 , and 1 mM DTT) and added to each well in a volume of $17.5\ \mu\text{L}$ for a final concentration in the $25\ \mu\text{L}$ mixture of 1.7 nM. After a 20 min preincubation at room temperature, the kinase reaction was initiated by the addition of $5\ \mu\text{L}$ of an activation mixture diluted in assay buffer containing biotinylated STKS1 and ATP for final concentrations of 50 nM biotinylated STKS1 and $5\ \mu\text{M}$ ATP. The plates were incubated for 30 min at room temperature and then stopped by the addition of $25\ \mu\text{L}$ of HTRF detection buffer containing phospho-STK antibody-Eu³⁺-cryptate and streptavidin labeled XL665 antibody at dilutions of 1:200 and 1:2647, respectively. Final assay dilutions of phospho-STK antibody-Eu³⁺-cryptate and streptavidin labeled XL665 antibody were 1:400 and 1:5294, respectively. Assay plates were incubated for 60 min at room temperature, and the plates were read on a Perkin-Elmer Envision multilabel plate reader (excitation of 320 nm, emission I of 665 nm, emission II of 615 nm).

PDK1 Assay. PDK1 activity was assayed using the PKA(Thr197) derived biotinylated peptide substrate, biotin-RTWT*LCG, and the AlphaScreen technology. Test compound and controls (*N*-[2-(diethylamino)ethyl]-5-[(*Z*)-(5-fluoro-2-oxo-1,2-dihydro-3*H*-indol-3-ylidene)methyl]-2,4-dimethyl-1*H*-pyrrole-3-carboxamide (sutent) and staurosporine) were prepared in 10% DMSO at 10-fold the desired final concentration and added to each well of a reaction plate (Corning 96-well half-area solid white nonbinding surface plate) in a volume of 2.5

μL . PDK1 was diluted in assay buffer (50 mM Tris, pH 8.0, 0.02 mg/mL BSA, 10 mM MgCl_2 , 1 mM EGTA, 10% glycerol, 0.1 mM Na_3VO_4 , 1 mM DTT) and added to each well in a volume of $17.5\ \mu\text{L}$ for a final concentration in the $25\ \mu\text{L}$ mixture of 6.0 nM. After a 20 min preincubation at room temperature, the kinase reaction was initiated by the addition of $5\ \mu\text{L}$ of an activation mixture diluted in assay buffer containing biotinylated PKA(Thr197), DOPS/DOPC, PtdIns(3,4,5)P3 and for final concentrations of $0.5\ \mu\text{M}$ biotinylated PKA(Thr197), $5.5\ \mu\text{M}$ DOPS, $5.5\ \mu\text{M}$ DOPC, $0.5\ \mu\text{M}$ PtdIns(3,4,5)P3, and $2\ \mu\text{M}$ ATP. The plates were incubated for 60 min at room temperature, and then the reaction was stopped in the dark by the addition of $10\ \mu\text{L}$ of stop/detection mixture prepared in assay buffer containing EDTA, AlphaScreen streptavidin donor and protein A acceptor beads, and phospho-AKT substrate antibody for final concentrations of 10 mM EDTA, 500 ng/well of both AlphaScreen streptavidin donor beads and protein A acceptor beads, and phospho-PKA C (Thr197) antibody at a final dilution of 1:945. Assay plates were incubated for 60 min at room temperature in the dark, and the plates were read on a Perkin-Elmer Envision multilabel plate reader (excitation wavelength of 640 nm, emission wavelength of 570 nm). All IC_{50} values reported are the geometric mean of at least $n = 2$ determinations.

Cellular Antiproliferation Assay (MTS). Antiproliferative cellular assays were conducted using the CellTiter nonradioactive cell proliferation assay developed by Promega utilizing the production of formazan from a tetrazolium compound by live cells. AN3CA and A2780 cells were obtained from ATCC. AN3CA cells were cultured in DMEM, and A2780 cells were cultured in RPMI supplemented with 10% FBS, 100 units/mL penicillin, 100 $\mu\text{g}/\text{mL}$ streptomycin, and 2 mM glutamine at 37°C under 5% CO_2 . Cells were plated in 96-well plates at 2000–10000 cells/well, cultured for 24 h, and treated with test compound to a final DMSO concentration no greater than 0.5% v/v for 72 h. PMS stock reagent (0.92 mg/mL in DPBS) was diluted 20-fold in MTS stock reagent (2 mg/mL in DPBS), and this MTS/PMS mixture was diluted 5-fold into each well of the 96-well plate. Plates were incubated for 3–4 h, and the absorbance of formazan was measured at 490 nm. Data were normalized to untreated controls. Dose response curves were fit to a four-parameter logistic equation, and IC_{50} values were determined. All IC_{50} values reported are the geometric mean of at least two independent determinations.

In Vitro Western Blot Pharmacodynamic Assay (p-Ser473, p-Thr308, p-PRAS40). Cellular activity was determined by measuring the phosphorylation status of Akt Ser473, Thr308, and its substrate phospho-PRAS40 using A2780 and AN3CA cell lines. A2780 and AN3CA cells were plated in six-well plates at 60–75% confluency and incubated at 37°C overnight in 5% CO_2 . At 75–90% confluency, cells were treated with test compound, following a 3-fold dilution scheme, for 1 h with a final DMSO concentration of less than 0.2% v/v. Cells were stimulated with 100 ng/mL EGF and 100 nM insulin for 15 min. The medium was removed, and $150\ \mu\text{L}$ of $1\times$ E-Page loading buffer (catalog no. EPBUF-01, Invitrogen) was added. Cells were scraped and transferred to a deep well 96-well plate and lysed by sonication at medium power four to six times in 30 s bursts. Samples were run on EPAGE gels and transferred to PVDF membranes using the iBlot system (Invitrogen). Membranes were washed for 3 min in distilled H_2O , blocked for 30 min in Odyssey blocking buffer (catalog no. 927-40000, LiCor), and then incubated overnight at 4°C in Odyssey blocking/TBST buffer (50 mM Tris, pH 7.4, 150 mM NaCl, 0.05% Tween 20) (1:3) with antibodies against phospho-Akt (catalog no. 9271 and catalog no. 9275, Cell Signaling Technology), phospho-PRAS40 (catalog no. 2640, Cell Signaling Technology), and β -actin (catalog no. A2228, Sigma). After three washes for 5 min each in TBST buffer, membranes were incubated with the appropriate secondary antibodies labeled with near-infrared or Alexa Fluor dyes (catalog no. 611-132-122 goat anti-rabbit IgG H + L, catalog no. 610-132-121 goat anti-mouse IgG H + L, Rockland catalog no. A21076 goat anti-rabbit IgG H + L, catalog no. A21057 goat anti-mouse IgG H + L, Molecular Probes). After 1 h of incubation, membranes were washed three times for 5 min each and then scanned using an Odyssey infrared scanner (LiCor). The intensity of the bands was quantified

using the accompanying software. Data were normalized to untreated controls. Dose response curves were fitted to a four-parameter logistic equation, and IC_{50} values were determined.

Cross-Species NADPH-Dependent Microsomal Stability Assay. Human and CD-1 mouse, liver microsomes (0.25 mg/mL), 3.3 mM $MgCl_2$, and NADPH-regenerating system (0.4 units/mL G6PDH, 1.3 mM NADP⁺, and 3.3 mM G6P) were incubated with 1 μ M compound for 0, 3, 6, 10, 15, or 30 min. The incubations were stopped with acetonitrile containing warfarin (internal standard), and the samples were analyzed by LC/MS/MS. Peak area ratios were used to determine percent remaining at each time point compared to time zero. Half-lives were estimated using the equation for monoexponential decay. Midazolam and propranolol (female mouse only) were used as positive controls.

CYP450 Inhibition Assay. Human liver microsomes (0.25 mg/mL), probe substrates [3 μ M midazolam (3A4), 5 μ M bufuralol (2D6), 100 μ M tolbutamide (2C9), 10 μ M paclitaxel (2C8), 80 μ M *S*-mephenytoin (2C19), and 50 μ M phenacetin (1A2)], 3.3 mM $MgCl_2$, 1 mM NADPH, and compound (0.1–10 μ M) dissolved in DMSO (0.1% final) were incubated for 10 min, at which time acetonitrile containing reserpine (internal standard) was used to stop the reaction. Solvents were evaporated under a constant stream of nitrogen gas at 35 °C and then reconstituted in 100 μ L of water for LC/MS/MS analysis. A cocktail of inhibitors was used as a positive control and consisted of 0.5 μ M ketoconazole (3A4), 1 μ M sulfaphenazole (2C9), 1 μ M quinidine (2D6), 2 μ M quercetin (2C8), 1 μ M nootkatone (2C19), and 0.5 μ M α -naphthoflavone (1A2). Incubations containing only DMSO (no compound) served as the 100% activity control. Percent inhibition was calculated based on the signal for the 100% activity control, and IC_{50} values were either estimated or determined using fit model 205 (one site dose response) in XLfit4 (Guildford, Surrey, U.K.).

Materials and Methods for in Vivo Studies. Six-week old NCr female nude mice were purchased from Taconic Farms (Germantown, NY) and allowed to acclimate for more than 2 weeks. Mice were housed in sterile microisolator cages, five mice per cage, and received food and water ad libitum.

In Vivo Pharmacokinetic Studies. Naive NCr female nude mice were utilized for a definitive PK study with compound **12e**. Oral administration (po) was at 100 mg/kg in NMP/DMA/Tween 80/PEG 400 (10:10:10:70). Time points for the oral arm were 0.5, 1, 2, 4, 8, 24, and 48 h after a single dose with three mice per time point. An iv arm (tail vein injection with a 27G needle) was administered at 2.5 mg/kg in DMA/propyleneglycol/cremophore/20% HPBCD in 0.2 M acetate buffer, pH 5.0 (10:30:10:50). Time points were 5, 15, 30 min and 1, 2, 4, 8, and 24 h after administration. The dosing volume for all groups was 10 mL/kg. At specific time points mice were euthanized with CO₂ inhalation. Whole blood was retrieved via cardiac puncture and placed in heparin coated tubes. Plasma was collected and placed on dry ice until analysis.

Acute Pharmacokinetic (PK) and Pharmacodynamic (PD) Assays in Vivo. AN3CA cells were purchased from ATCC. Cells were cultured in sterile RPMI supplemented with 10% fetal bovine serum. Mice were implanted subcutaneously in the upper right shoulder flank with 5×10^6 cells suspended in sterile Hanks buffered salt solution (HBSS) in 0.2 mL volume. Mice were monitored and randomized when tumor size ranged between 300 and 500 mg. Tumor measurements and body weights were collected once with electronic calipers and balance. The tumor weight (mg) was calculated from the following equation: [(length)(width)²]/2. This formula was also used to calculate tumor volume, assuming unit density 1 mg = 1 mm³. Mice received a single administration of selected compound dissolved in NMP/DMA/Tween 80/PEG400 (10:10:10:70) or 0.1% Tween 80 in 1% HPMC. Dosing volume was 10 mL/kg. At designated time points after administration, mice were euthanized with CO₂ inhalation and tumor tissue was trisected. Two-thirds went immediately into tubes on dry ice, while one-third was placed in 10% formalin for further analysis. Whole blood was harvested via cardiac puncture and placed in heparin coated tubes. Plasma was retrieved and placed in an Eppendorf tube on dry ice until analysis.

Determination of **12j and **12e** Concentrations in Mouse Plasma and AN3CA Tumors.** CD-1 mouse plasma (sodium heparin as anticoagulant) from Bioreclamation (Hicksville, NY) was used for standard curve preparation and plasma sample dilution when necessary. Tumor tissues (density was treated as 1 mg/mL) were weighed and diluted with 10 mM NH₄OAc at volumes 9× the tumor volume (i.e., 450 μ L buffer was added to a 50 mg tumor). The mixtures were homogenized using a hand-held homogenizer, and vehicle treated mouse tissue homogenates were used to prepare standard curves. Plasma and tissue standards were prepared by spiking 5 μ L of 10× acetonitrile spiking solutions into 50 μ L of plasma or tumor tissue to produce standards from 1 to 2000 ng/mL concentrations. Study plasma samples (5 μ L) were diluted with 45 μ L (1:10) of blank mouse plasma. A total of 50 μ L plasma was added to 400 μ L of acetonitrile containing 50 ng/mL reserpine (internal standard). Tumor homogenate (50 μ L) was added without further dilution to 400 μ L of acetonitrile containing 50 ng/mL reserpine. The mixtures were vortexed, sonicated for 2 min, and then centrifuged at 3000 rpm for at least 10 min. Supernatant (200 μ L) was transferred to a shallow 96-well plate and solvent removed under nitrogen gas, 30 °C. The dried samples were reconstituted in 150 μ L of 10% acetonitrile in HPLC water for LC/MS/MS analysis.

LC/MS/MS Analysis of Plasma and Tumor Samples. Analysis was performed using a Waters Quattro Micro triple quadrupole mass spectrometer (Milford, MA) equipped with an ESI source. The samples were delivered to the mass spectrometer ion source by an Agilent 1100 binary HPLC pump (Santa Clara, CA), and samples were injected using a LEAP CTC PAL autoinjector (Carrboro, NC). A Waters SymmetryShield RP18 (2.1 mm × 100 mm, 3.5 μ m, Milford, MA) reverse-phase HPLC column was used for separation. Mobile phases contained water (A) and acetonitrile (B) both modified with 0.1% formic acid. The HPLC gradient was started and maintained at 10% mobile phase A for the first 0.5 min and was increased to 80% mobile phase B over the next 6.5 min and held there for 0.8 min. At 7.81 min, the mobile phase was returned to 10% mobile phase A and maintained there until the end of the run at 10 min. Flow rates were set at 0.2 mL/min. Transitions ions monitored were as follows: for **12j** they were m/z 572.1 → 391.0, 432.9, and 530.0 (all three summed for quantification); for **12e** they were m/z 498.0 → 272.2 and 377.2 (both summed for quantification); for reserpine it was m/z 609.2 → 195.2. Peak areas for all analytes and the internal standard (reserpine) were determined using Waters MassLynx, version 4.1, software (Waters, Milford, MA). Peak area ratios were next calculated by dividing the peak area of analyte by the reserpine peak area for all test samples. Standard curves were fit with a linear equation and with weighting of $1/x^2$. All R^2 values for linear fit for plasma and tissues were >0.98. When appropriate, AUC values were estimated with the linear trapezoidal method using WinNonlin (version 5.2) to calculate oral bioavailability.

Pharmacodynamic Analysis of the Akt Pathway in Vivo (p-Ser473, p-Thr308, p-P70s6). Frozen tumor tissues were ground in mortars with liquid nitrogen. The tissue powder was lysed in buffer consisting of 50 mM Tris-HCl (pH 7.5), 20 mM NaCl, 6 mM EDTA, 15 mM EGTA, 1% NP-40, and a protease/phosphatase inhibitor cocktail. Samples were run on EPage gels and transferred to PVDF membranes using the iBlot system (Invitrogen). Membranes were washed for 3 min in distilled H₂O, blocked for 30 min in Odyssey blocking buffer (catalog no. 927-40000, LiCor), and then incubated overnight at 4 °C in Odyssey blocking/TBST buffer (50 mM Tris, pH 7.4, 150 mM NaCl, 0.05% Tween 20) (1:3) with antibodies against phospho-Akt (Ser473 and Thr308) (catalog no. 9271 and catalog no. 9275, Cell Signaling Technology), phospho-p70s6 (Thr389) (catalog no. 9206, Cell Signaling Technology), and β -actin (catalog no. A2228, Sigma). After three washes for 5 min each in TBST buffer, membranes were incubated with the appropriate secondary antibodies labeled with near-infrared or Alexa Fluor dyes (catalog no. 611-132-122), goat anti-rabbit IgG H + L (catalog no. 610-132-121), goat anti-mouse IgG H + L (Rockland or catalog no. A21076), goat anti-rabbit IgG H + L (catalog no. A21057), goat anti-mouse IgG H + L (Molecular Probes). After 1 h of incubation, membranes were washed three times for 5 min

each and then scanned using the Odyssey infrared scanner (LiCor). The intensities of the bands were quantitated using the accompanying software.

Crystallization, Data Collection, and Refinement. A 6xHis-Akt1 (2–446) with a TEV protease site construct was cloned in a baculovirus vector and expressed in Sf9 cells. To aid the crystallization, three mutations were introduced on the linker region (E114A, E115A, and E116A) in the Akt1 (2–446) construct. The protein was purified with a similar protocol as described for the Akt isoforms described above and the 6xHis tag was removed using TEV protease. Cocrystals of 12j were obtained with the following conditions: 16% butanol, 10 mM ammonium sulfate, 0.1% 2-mercaptoethanol, 15% ethylene glycol, 50 mM Tris, pH 7.5. Diffraction data were collected at NSLS on the X29 beamline, and the data were processed using Mosflm and scaled using Scala. The structure was solved by molecular replacement using the Phaser program with search models consisting of Akt2 (1MRV) and the Akt1 PH domain (2UVM). The initial model was built using ARP/wARP program, and the model was subsequently improved through iterative cycles of manual model building with Coot and refinement with ARP/wARP or Refmac5.

AUTHOR INFORMATION

Corresponding Author

*Phone: (781) 994-0467. E-mail: tchan@arqule.com.

Notes

The authors declare no competing financial interest.

ABBREVIATIONS USED

PI3K/Akt/mTOR, phosphoinositide 3-kinase/protein kinase B/mammalian target of rapamycin; PH, pleckstrin homology; HM, hydrophobic motif; AMP-PNP, adenylyl imidodiphosphate, tetralithium salt; HCl, hydrochloric acid; HBTU, O-benzotriazole-*N,N,N',N'*-tetramethyluronium hexafluorophosphate; CDI, 1,1'-carbonyldiimidazole; EDCI, 1-(3-dimethylaminopropyl)-3-ethylcarbodiimide; NaOH, sodium hydroxide; T_m , protein melting temperature; STD, standard deviation; MTS, [3-(4,5-dimethylthiazol-2-yl)-5-(3-carboxymethoxyphenyl)-2-(4-sulfophenyl)-2H-tetrazolium, inner salt; PRAS40, proline-rich Akt substrate, 40 kDa; p70S6, ribosomal protein S6 kinase; SPR, surface plasmon resonance; IA-MS, indirect affinity mass spectrometry; SEC/LC/MS, size exclusion/liquid chromatography/mass spectrometry; TSA, thermal shift assay, MLM, mouse liver microsome; HLM, human liver microsome; K_d , dissociation constant

REFERENCES

- (1) Liu, P.; Cheng, H.; Roberts, T. M.; Zhao, J. J. Targeting the Phosphoinositide 3-Kinase Pathway in Cancer. *Nat. Rev. Drug Discovery* **2009**, *8*, 627–644.
- (2) Lindsley, C. W. The Akt/PKB Family of Protein Kinases: A Review of Small Molecule Inhibitors and Progress towards Target Validation: A 2009 Update. *Curr. Top. Med. Chem.* **2010**, *10*, 458–477.
- (3) Fresno-Vara, J. A.; Casado, E.; de-Castro, J.; Cejas, P.; Beldaniesta, C.; Gonzalez-Baron, M. PI3K/Akt Signalling Pathways and Cancer. *Cancer Treat. Rev.* **2004**, *30*, 193–204.
- (4) Collins, I. Targeting Small-Molecule Inhibitors of Protein Kinase B as Anticancer Agents. *Anti-Cancer Agents Med. Chem.* **2009**, *9*, 32–50.
- (5) Hirai, H.; Sootome, H.; Nakatsuru, Y.; Miyama, K.; Taguchi, S.; Tsujioka, K.; Ueno, Y.; Hatch, H.; Majumder, P. K.; Pan, B.-S.; Kotani, H. MK-2206, an Allosteric Akt Inhibitor, Enhances Antitumor Efficacy by Standard Chemotherapeutic Agents or Molecular Targeted Drugs in Vitro and in Vivo. *Mol. Cancer Ther.* **2010**, *9*, 1956–1967.
- (6) Eathiraj, S.; Palma, R.; Volckova, E.; Hirschi, M.; France, D. S.; Ashwell, M. A.; Chan, T. C. K. Discovery of a Novel Mode of Protein Kinase Inhibition Characterized by the Mechanism of Inhibition of

Human Mesenchymal-Epithelial Transcription Factor (c-Met) Protein Autophosphorylation by ARQ 197. *J. Biol. Chem.* **2011**, *286*, 20666–20676.

- (7) Eathiraj, S.; Palma, R.; Hirschi, M.; Volckova, E.; Enkeleda, N.; Castro, J.; Chen, C.-R.; Chan, T. C. K.; France, D. S.; Ashwell, M. A. A Novel Mode of Protein Kinase Inhibition Exploiting Hydrophobic Motifs of Autoinhibited Kinases. *J. Biol. Chem.* **2011**, *286*, 20677–20687.

- (8) Calleja, V.; Alcor, D.; Laguerre, M.; Park, J.; Vojnovic, B.; Hemmings, B. A.; Downward, J.; Parker, P. J.; Larijani, B. Intramolecular and Intermolecular Interactions of Protein Kinase B Define Its Activation in Vivo. *PLoS Biol.* **2007**, *5*, e95.

- (9) Huang, X.; Begley, M.; Morgenstern, K. A.; Gu, Y.; Rose, P.; Zhao, H.; Zhu, X. Crystal Structure of an Inactive Akt2 Kinase Domain. *Structure* **2003**, *11*, 21–30.

- (10) Muckenschnabel, I.; Falchetto, R.; Mayr, L. M.; Filipuzzi, I. SpeedScreen: Label-Free Liquid Chromatography–Mass Spectrometry-Based High-Throughput Screening for the Discovery of Orphan Protein Ligands. *Anal. Biochem.* **2004**, *324*, 241–249.

- (11) Lo, M. C.; Aulabaugh, A.; Jin, G.; Cowling, R.; Bard, J.; Malamas, M.; Ellestad, G. Evaluation of Fluorescence-Based Thermal Shift Assays for Hit Identification in Drug Discovery. *Anal. Biochem.* **2004**, *332*, 153–159.

- (12) Pantoliano, M.; W., Petrella, E. C.; Kwasnoski, J. D.; Lobanov, V. S.; Myslik, J.; Graf, E.; Carver, T.; Asel, E.; Springer, B. A.; Lane, P.; Salemme, F. R. High-Density Miniaturized Thermal Shift Assays as a General Strategy for Drug Discovery. *J. Biomol. Screening* **2001**, *6*, 429–440.

- (13) Nordin, H.; Jungnelius, M.; Karlsson, R.; Karlsson, O. P. Kinetic Studies of Small Molecule Interactions with Protein Kinases Using Biosensor Technology. *Anal. Biochem.* **2005**, *340*, 359–368.

- (14) Bozulic, L.; Hemmings, B. A. PIKKing on PKB: Regulation of PKB Activity by Phosphorylation. *Curr. Opin. Cell Biol.* **2009**, *21*, 256–261.

- (15) All 3-(3*H*-imidazo[4,5-*b*]pyridin-2-yl)pyridin-2-amine analogues tested in the two counterscreens had IC₅₀ values greater than 10 μM.

- (16) Chang, L. C. W.; Künzel, J. K. F. D.; Mulder-Krieger, T.; Westerhout, J.; Spangenberg, T.; Brussee, J.; IJzerman, A. P. 2,6,8-Trisubstituted 1-Deazapurines as Adenosine Receptor Antagonists. *J. Med. Chem.* **2007**, *50*, 828–834.

- (17) Hu, B.; Jetter, J.; Kaufman, D.; Singhaus, R.; Bernotas, R.; Unwalla, R.; Quinet, E.; Savio, D.; Halpern, A.; Basso, M.; Keith, J.; Clerin, V.; Chen, L.; Qiang-Yuan Liu, Q.-Y.; Feingold, L.; Huselton, C.; Azam, F.; Goos-Nilsson, A.; Wilhelmsson, A.; Nambir, P.; Wrobela, J. Further Modification on Phenyl Acetic Acid Based Quinolines as Liver X Receptor Modulators. *Bioorg. Med. Chem.* **2007**, *15*, 3321–3333.

- (18) Ben-zeev, E.; Chen, D.; Fichman, M.; Ghosh, S.; Koerner, S.; Lin, J.; Marantz, Y.; Melendez, R.; Mohanty, P.; Shacham, S.; Zhang, Z. Carboxamide Compounds as Chemokine Receptor Agonists. PCT WO2009/076512 A1, 2009.

- (19) Luo, Y.; Shoemaker, A. R.; Liu, X.; Woods, K. W.; Thomas, S. A.; de Jong, R.; Han, E. K.; Li, T.; Stoll, V. S.; Powlas, J. A.; Oleksijew, A.; Mitten, M. J.; Shi, Y.; Guan, R.; McGonigal, T. P.; Klinghofer, V.; Johnson, E. F.; Levenson, J. D.; Bouska, J. J.; Mamo, M.; Smith, R. A.; Gramling-Evans, E. E.; Zinker, B. A.; Mika, A. K.; Nguyen, P. T.; Oltersdorf, T.; Rosenbert, S. H.; Li, Q.; Giranda, V. L. Potent and Selective Inhibitors of Akt Kinases Slow the Progress of Tumors in Vivo. *Mol. Cancer Ther.* **2005**, *4*, 977–986.

- (20) Ashwell, M. A.; Palma, R.; Eathiraj, S. Use of Crystal Structures of Kinase Complexes with Inhibitors in the Design of Novel Inhibitor Drugs. US 7960134, 2011.

- (21) Compounds were tested at a single concentration against a panel of 33 kinases (MSK1, MSK2, P70S6KB1, PDK1, PKA, PKC-α, PKC-β1, PKC-ETA, PKC-γ, PKC-THETA, PRKX, ROCK1, RSK1, RSK2, RSK3, RSK4, SGK1, SGK2, SGK3, CAMK2δ, MAPKAPK2, PIM-1, CDK1/cyclinB, CDK2/cyclinE, CDK5/p35, MAPK3, PAK2, PAK3, FGFR1, FMS, INSR, RET, TIE2) specifically focused on the AGC group of kinases in addition to a selection of targets across the kinase diversity. The reference standard staurosporine was included

as an internal control. The assays were performed on the Caliper microfluidics platform under consistent assay conditions using a fluorescently labeled peptide substrate. Compounds were tested in duplicate at a 5 μM final concentration.

(22) Kovacina, K. S.; Park, G. Y.; Bae, S. S.; Guzzetta, A. W.; Schaefer, E.; Birnbaum, M. J.; Roth, R. A. Identification of a Proline-Rich Akt Substrate as a 14-3-3 Binding Partner. *J. Biol. Chem.* **2003**, *278*, 10189–10194.

(23) Lindsley, C. W.; Zhao, Z.; Leister, W. H.; Robinson, R. G.; Barnett, S. F.; Defeo-Jones, D.; Jones, R. E.; Hartman, G. D.; Huff, J. R.; Huber, H. E.; Duggan, M. E. Allosteric Akt (PKB) Inhibitors: Discovery and SAR Isozyme Selective Inhibitors. *Bioorg. Med. Chem. Lett.* **2005**, *15*, 761–764.

(24) The crystallographic data described here has been deposited with the Protein Data Bank (PDB code for **12j**: 4EJN).

(25) Wu, W.-I.; Voegtli, W. C.; Sturgis, H. L.; Dizon, F. P.; Vigers, G. P. A.; Brandhuber, B. J. Crystal Structure of Human AKT1 with an Allosteric Inhibitor Reveals a New Mode of Kinase Inhibition. *PLoS One* **2010**, *5* (9), e12913.

(26) The inhibition of 297 kinases by **12j** was characterized by screening at Carna Biosciences. At 1 μM , no kinase was inhibited more than 17%.